Secondary reactions of aromatics-derived oxygenated organic molecules lead to plentiful highly oxygenated organic molecules within an intraday OH exposure

Yuwei Wang[1], Chuang Li[1], Ying Zhang[1], Yueyang Li[1], Gan Yang[1], Xueyan Yang[1], Yizhen Wu[1], Lei Yao[1,2], Hefeng, Zhang[3*], Lin Wang[1,2,4,5,6 *]

[1] Shanghai Key Laboratory of Atmospheric Particle Pollution and Prevention (LAP[3]), Department of Environmental Science and Engineering, Jiangwan Campus, Fudan University, Shanghai 200438, China

[2] Shanghai Institute of Pollution Control and Ecological Security, Shanghai 200092, China

[3] State Environmental Protection Key Laboratory of Vehicle Emission Control and Simulation, Vehicle Emission Control Center of Ministry of Ecology and Environment, Chinese Research Academy of Environmental Sciences, Beijing 100012, China

[4] IRDR International Center of Excellence on Risk Interconnectivity and Governance on Weather/Climate Extremes Impact and Public Health, Fudan University

[5] National Observations and Research Station for Wetland Ecosystems of the Yangtze Estuary, Shanghai, China

[6] Collaborative Innovation Center of Climate Change, Nanjing, 210023, China

** Corresponding Author: H.Z., email, zhanghf@craes.org.cn; phone, +86-10-84915586*

L.W., email, lin_wang@fudan.edu.cn; phone, +86-21-31243568

ABSTRACT. Highly oxygenated organic molecules (HOMs) can participate in new particle formation (NPF) and enhance growth of newly formed particles partially because of their low volatility. Previous studies have shown formation of HOMs via autoxidation reactions of RO_2 intermediates generated by OH-initiated oxidation of anthropogenic volatile organic compounds (VOCs). It was also suggested that multi-generation OH oxidation could be an important source for aromatics-derived HOMs. However, our understanding on the generation of aromatics-derived HOMs are still insufficient, especially for their formation mechanisms, which determine molar yields of HOMs and are essential to the establishment of global chemical box models related to HOMs. In this study, with a potential aerosol mass oxidation flow reactor (PAM OFR), two series of OH-initiated oxidation experiments of 1,3,5-trimethylbenzene (1,3,5-TMB) were conducted to investigate the formation of aromatics-derived HOMs. In the first series, the evolution of oxidation products of 1,3,5-TMB in an OH exposure range of $(0.5 – 5.0)\times10^{10}$ molecules cm^{-3} s, equivalent to an OH exposure of 0.7 – 6.9 hours at an OH concentration ([OH]) of 2×10^6 molecules cm^{-3}, was investigated by a nitrate-based chemical ionization mass spectrometer and a Vocus proton-transfer-reaction mass spectrometer, indicating significant secondary OH chemistry during the ageing of stabilized

first generation oxygenated products within an intraday OH exposure and formation of various HOMs with lower double bond equivalence (DBE). In addition, organonitrates, formed after the introduction of NO_x into the reaction systems, further confirmed the existence of such secondary reactions. The second series of experiments was conducted with same residence time but much lower [OH], which also shows the generation of multi-generation HOMs with an [OH] as low as 1.06×10^7 molecules cm^{-3} for 53 s, i.e., an OH exposure of around 5.86×10^8 molecules cm^{-3} s. Our study suggests an important role of secondary OH chemistry in the oxidation of aromatics, if these oxygenated products survived long enough in the ambient, and elucidates detailed formation mechanisms of certain HOM products.

1 Introduction

OH radicals can react with volatile organic compounds (VOCs) in the atmosphere, converting primary pollutants to secondary ones. Generated from oxidation of VOCs, oxygenated organic molecules (OOMs) are crucial in a variety of atmospheric chemical processes, contributing efficiently to the formation of secondary organic aerosols (SOAs) and ground-level O_3 (Ng et al., 2010; Wang et al., 2022; Qu et al., 2021). Among the enormous number of oxygenated VOCs (OVOCs), highly oxygenated organic molecules (HOMs) have recently attracted significant attention (Bianchi et al., 2019). Most of HOMs are low volatility organic compounds (LVOCs) or extremely low volatility organic compounds (ELVOCs), and thus are able to drive the initial formation of nucleated particles under certain conditions and contribute to the subsequent growth of newly-formed particles, which finally enhance SOA formation (Tröstl et al., 2016; Lehtipalo et al., 2018; Stolzenburg et al., 2018; Mohr et al., 2019; Qiao et al., 2021).

Formation of HOMs is triggered by oxidation of VOCs in the gas phase. Peroxy radicals (RO_2) are generated at the initial step and will undergo an intramolecular hydrogen atom shift forming a hydroperoxide functionality and an alkyl radical. A molecular oxygen will rapidly attach to this alkyl radical and form a new and more oxidized RO_2. This reaction is called as autoxidation and the newly formed RO_2 can go through another autoxidation or bimolecular termination reactions to form a stabilized product (Crounse et al., 2013). Autoxidation is suggested to be responsible for widely detected HOMs in the atmosphere, because it can form highly oxygenated RO_2 in a short time scale. In terms of biomolecular reactions, RO_2 reacts appreciable only with hydroperoxyl radical (HO_2), NO, and another RO_2. The RO_2 reaction chain in polluted areas is largely terminated by NO, which prohibits generation of compounds with high oxidation levels and reduces yields of HOMs (Bianchi et al., 2019).

Nevertheless, autoxidation reactions alone are not enough to explain the large numbers of oxygen atoms and low double bond equivalence (DBE, calculated as $nC - \frac{nH+nN}{2} + 1$ where nC, nH, and nN stand for the number of carbon, hydrogen, and nitrogen atoms, respectively, in a molecular) for HOMs observed in laboratory experiments and ambient campaigns. Take alkylbenzenes as an example, previous studies suggest that the main products of OH-initiated oxidation of alkylbenzenes (C_xH_{2x-6}, x=7, 8, or 9), i.e., bicyclic peroxy radicals (BPR, $C_xH_{2x-5}O_5$·, x=7, 8, or 9) (Jenkin et al., 2003), can undergo an autoxidation reaction and form a new peroxy radical, $C_xH_{2x-5}O_7$· (x=7, 8, or 9) (Wang et al., 2017).Autoxidation of BPR could be very fast if it has a favorable structure, as found in a previous study (Wang et al., 2017). On the other hand, the structure of the resulting $C_xH_{2x-5}O_7$· is strongly different from that of BPR, whose autoxidation reaction rate can be as low as the order of 0.001 s^{-1}, since it lacks enhancements from favorable transition state geometries and substitutes or resonance structures (Bianchi et al., 2019; Otkjær et al., 2018). Such a slow autoxidation reaction rate cannot explain the extensive existence of HOM monomers with more than 7 oxygen atoms and HOM dimers with more than 10 oxygen atoms, which are the maximum numbers of oxygen atoms in stabilized first generation monomer and dimer products, respectively, formed from $C_xH_{2x-5}O_7$· (Molteni et al., 2018; Wang et al., 2020b; Mentel et al., 2015; Berndt et al., 2018b). Another possibility is the formation of a second oxygen bridge after the hydrogen shift of BPR (Molteni et al., 2018), but this reaction pathway would not allow a further oxygenation reaction without a breakage of the carbon ring, which is also unpromising. A very recent investigation offers new insights into the formation mechanism of these products, indicating the molecular rearrangement of BPR can initiate a series of autoxidation (Iyer et al., 2023). However, the formation mechanism of HOMs with a large hydrogen atom number, i.e., low DBE, is still vague. For example, monomer products with 16 hydrogen atoms in the OH-initiated oxidation of TMB and those with 14 hydrogen atoms in the OH-initiated oxidation of xylene were observed in the laboratory, both with a DBE of 2 lower than their precursors' (Molteni et al., 2018), but their formation mechanisms cannot be explained by any known mechanisms with only one OH attack.

Multigeneration reactions of VOCs complicate HOMs' formation. Previous studies indicate that HOMs can also be formed by sequential oxidation of stabilized first-generation products of benzene and toluene (Garmash et al., 2020; Cheng et al., 2021). Garmash et al. (2020) conducted OH oxidation experiments of benzene and toluene with an OH exposure equivalent to atmospheric oxidation times of 10 hours – 15 days at OH concentrations of ~10^6 molecules cm^{-3}. Cheng et al. (2021) simulated oxidation of benzene and toluene with an OH exposure equivalent to 2.4 – 19.4 days of atmospheric photochemical ageing. Certainly, such

extremely high OH exposures favor secondary OH chemistry and help to facilitate our understanding on product distributions, but such a long timescale limits atmospheric implications of their results, given the complex physical and chemical processes that occur at night.

Compared to benzene and toluene, trimethylbenzene (TMB) is a compound characterized with much larger HOM molar yields when reacted with OH, and the abundance of TMB in the atmosphere is unignorable (Molteni et al., 2018; Yuan et al., 2012). Previous laboratory experiments on TMB-derived HOMs mainly focused on the autoxidation reactions of BPR and the influences of NO_x, and the quantity of experiments was very finite, restricting the application of their conclusions to atmospheric relevant conditions (Tsiligiannis et al., 2019; Wang et al., 2020b). From the mechanism perspective, a number of HOM monomers with more than 7 oxygen atoms detected in the OH-initiated oxidation of TMB were previously assumed to be generated via multiple autoxidation reactions (Molteni et al., 2018). Nevertheless, a subsequent OH oxidation of the first-generation oxygenated products might be more plausible for the formation of HOM monomers with more than 7 oxygen atoms from the present point of view. Indeed, laboratory experiments show that RO_2 formed during the second-generation OH oxidation of the stabilized first-generation oxidation products can also undergo autoxidation reactions, which entangles reaction mechanisms potentially involved in the formation of those HOMs and justifies more investigations on the multigeneration OH oxidation of aromatics (Wang et al., 2020b). Atmospheric OH concentration ([OH]) up to 6×10^6 – 2.6×10^7 molecule cm^{-3}, which is several times higher than the typical average atmospheric [OH], 1.5×10^6 molecule cm^{-3} (Jacob, 1999), has been frequently observed in both urban and suburban environments in China (Tan et al., 2019; Lu et al., 2012), leading to a realistic implication of multigeneration OH oxidation. Therefore, it is imperative to study chemical characteristics of aromatics-derived HOMs at different OH exposures, especially those that are less than or equivalent to one day of atmospheric oxidation.

In this study, two series of laboratory experiments on OH-initiated oxidation of 1,3,5-TMB, selected as an example of anthropogenic VOCs, were conducted. One was conducted with [OH] ranging from 9.32×10^7 to 1.03×10^9 molecule cm^{-3}, corresponding to an OH exposure equivalent to atmospheric oxidation times of roughly 0.7 – 6.9 hours at an average daytime [OH] of 2.0×10^6 molecules cm^{-3}. A nitrate-based chemical ionization mass spectrometer (nitrate CIMS) and a Vocus proton-transfer-reaction mass spectrometer (Vocus PTR) were deployed to measure the oxidation products and the precursor, respectively. We explored the evolution of oxidation products to investigate the secondary OH chemistry of stabilized first-generation oxidation products generated by the oxidation of 1,3,5-TMB. Furthermore, the influence of NO on the

formation of HOMs was investigated by introducing N_2O into the reaction system. In addition, another series of experiments under atmospheric relevant [OH] were conducted to confirm the applicability of the above-developed multi-generation OH oxidation mechanisms in the ambient atmosphere.

2 Methods

OH-initiated oxidation of 1,3,5-TMB was investigated in a potential aerosol mass oxidation flow reactor (PAM OFR) system at T = 298 ± 1 K and a pressure of 1 atm (Lambe et al., 2015). Two series of experiments were conducted, one under high [OH] conditions and the other under low [OH] conditions. Hereafter, we refer to the series of high [OH] experiments as 'the 1st-round experiments' and the low [OH] ones as 'the 2nd-round experiments', respectively. The i^{th} experiment in the 1st-round experiments is labelled as 1-i and the one in the 2nd-round experiments as 2-i, where i stands for its serial number. The experimental settings in this study differed slightly from what were used previously (Wang et al., 2020b). In the 1st-round experiments, forty OH experiments without NO_x (Exp. 1-1 – 1-40) and twenty-eight experiments with NO_x (Exp. 1-41 – 1-68) were performed. Seven experiments were conducted in the 2nd-round, four without NO_x (Exp. 2-1 – 2-4) and three with NO_x (Exp. 2-5 – 2-7). The experimental conditions are summarized in Table S1, including concentrations of the precursor, ozone, and NO and NO_2. The equivalent OH exposure in the OFR for each experiment was estimated according to the precursor consumption, and also listed in Table S1. OH exposures in the OFR were in the range of $(5.2 – 48.7)\times10^9$ and $(0.6 – 5.5)\times10^9$ molecules cm^{-3} s in the 1st-round and 2nd-round experiments, respectively.

A home-made 1,3,5-TMB/N_2 cylinder was used as a stable gaseous precursor source in the experiments, from which the flow rate of 1,3,5-TMB/N_2 varied between 1 – 3 sccm (standard cubic centimeter per minute), leading to $7.08\times10^{11} – 1.54\times10^{12}$ molecule cm^{-3} of 1,3,5-TMB in the 1st-round experiments, and 7.55×10^{11} or 8.45×10^{11} molecule cm^{-3} of 1,3,5-TMB in the 2nd-round experiments, respectively (Table S1). A total flow of 15 slpm (standard liters per minute) zero-gas generated by a zero-gas generator (model 737-13, Aadco Instruments Inc.), together with the 1,3,5-TMB/N_2 flow, was introduced into the OFR. The reaction time in both series of experiments was kept at around 53 s and the flow reactor was kept as a plug flow one in both series. The flow in the PAM OFR is laminar with a very low axial mixing, as characterized with a Taylor dispersion model in a previous study (Lambe et al., 2011). 6 slpm out of the 15 slpm zero-gas was initially passed through a Nafion humidifier (Perma Pure Model FC100-80-6MSS) filled with ultra-pure water and finally converged with the main flow into the OFR to achieve and keep a desired RH of 20.0 ± 2.5 % in the OFR throughout all the experiments, and

2 slpm was initially passed through a separate ozone chamber, resulting in an initial ozone concentration of around 1.05×10^{13} – 2.16×10^{13} molecule cm^{-3} in the OFR in the 1st-round experiments and 3.01×10^{12} – 3.72×10^{12} molecule cm^{-3} in the 2nd-round experiments, respectively. The OFR was operated with only the 254 nm lights on, under which the primary oxidant production reactions in the OFR were $O_3 + hv\,(254\,nm) \rightarrow O_2 + O(^1D)$ and $O(^1D) + H_2O \rightarrow 2OH$. After turning on of UV lights, a HOM compound is believed to be generated if its signal is more than 3 standard deviations of its background signal. If the fluctuations in the 1-min-averaged signals of both TMB in the Vocus PTR and typical HOMs (i.e., $C_9H_{14}O_7(NO_3)^-$) in the nitrate CIMS are within 2% during a 10-min period, a steady state was assumed to be reached. It usually took around no more than 2 minutes for the signals of HOMs to stabilize after the adjustment of UV lights. We typically monitored the reaction products for around 20 minutes for each experiment. An ozone monitor (Model 106-M, 2B technologies) and a trace-gas analyzer for NO-NO_2-NO_x (Thermo, 42i-TL) were placed at the exit of the OFR to measure concentrations of ozone and NO_x, respectively.

Non-tropospheric VOC and OVOC photolysis is a typical issue that should be taken into account when evaluating the OFR settings, especially under the high UV light dose settings in the 1st-round experiments. Our evaluation on photolysis of the precursor and HOMs shows that photolysis was not a contributor to our observation on C9 and C18 HOM formation. The photolysis rate of 1,3,5-TMB can be estimated based on the absorption cross-sections of 1,3,5-TMB at 254 nm (Keller-Rudek et al., 2013) and UV photon fluxes estimated by a chemistry model discussed in the following sections. The ratio of photolysis-to-OH reaction for 1,3,5-TMB in our 1st-round experiments was merely 0.010 – 0.033. Hence, photolysis of 1,3,5-TMB was insignificant in the OFR. For stabilized products such as C9 and C18 HOMs, the cross sections of organic molecules are usually ~ 3.9×10^{-18} – 3.9×10^{-17} cm^2 (Peng et al., 2016), while the reaction rate between OH and the stabilized first-generation products are estimated to be around 1.28×10^{-10} $molecule^{-1}$ cm^3 s^{-1}, as suggested by Master Chemical Mechanism (MCM) (Jenkin et al., 2003). Hence, the ratio of photolysis rates of C9 and C18 HOMs to their secondary OH oxidation rates is estimated to be around 0.020 – 0.056 in the 1st-round experiments. In the 2nd-round, the influences of photolysis should be even lower due to the much lower light intensity.

For experiments with NO_x in the 1st-round experiments, 350 sccm N_2O (99.999%, Air Liquid) was added into the OFR to produce and sustain NO_x mixing ratios at levels that were sufficiently high to be a competitive sink for RO_2 radicals. NO and NO_2 were produced via the reaction $N_2O + O(^1D) \rightarrow 2NO$, followed by the reaction $NO + O_3 \rightarrow NO_2 + O_2$. Two sets of irradiance intensities were chosen for NO_x experiments, generally resulting in two NO_x levels,

4.41×10^{10} molecule cm^{-3} NO + 1.72×10^{12} molecule cm^{-3} NO_2 (Exp. 1-41 – 1-54) and 1.18×10^{11} molecule cm^{-3} NO + 2.94×10^{12} molecule cm^{-3} NO_2 (Exp. 1-55 – 1-68) at the exit of the OFR. With the aim to slightly modify OH exposure but keep NO_x concentrations constant among each set of experiments, the initial concentrations of 1,3,5-TMB were adjusted in a large range from 4.09×10^{11} to 2.06×10^{12} molecule cm^{-3} while RH and irradiances were not changed, as an increase in the precursor concentration corresponds to a larger sink for OH. In the 2nd-round experiments, due to the lower $O(^1D)$ in the PAM OFR, 2.5 slpm pure N_2O was utilized instead, whereas the total flow rate was kept the same as that in the 1st-round. We lowered the light intensity to obtain a lower [OH] in the PAM OFR, which also resulted in fluctuations in the NO concentrations ([NO]) from 3.19×10^{10} to 1.74×10^{11} molecule cm^{-3} and the NO_2 concentrations ($[NO_2]$) from 2.70×10^{11} to 9.31×10^{11} molecule cm^{-3}.

A nitrate CIMS (Ehn et al., 2014; Eisele and Tanner, 1993) and a Vocus PTR (Krechmer et al., 2018) were deployed at the exit of the OFR to measure the oxidation products of 1,3,5-TMB in the 1st-round experiments. These two mass spectrometers have been well characterized in a previous study (Wang et al., 2020b).

The sample flow rate for the nitrate CIMS in the 1st round-experiments was 8 slpm through a Teflon tube with an outer diameter (OD) of 1/4 in. and a length of 70 cm. The sheath flow for the nitrate CIMS was supplied by a zero-gas generator at a flow rate of 15 slpm. Mass resolution was approximately 8000 for ions with m/z larger than 200 Th. HOMs generated from TMB oxidation were charged in the ambient pressure interface region by collisions with nitrate clusters, $(HNO_3)_x \cdot NO_3^-$ (x = 0 – 2), and detected by nitrate CIMS as clusters with NO_3^-, i.e., $HOM \cdot NO_3^-$ (Hyttinen et al., 2015). In addition, HOMs' signals were corrected with relative transmission efficiencies of our nitrate CIMS (Heinritzi et al., 2016). We followed the same sampling method of PAM OFR as those in previous studies, in order to obtain a similar flow tube residence time distributions (RTDs) and thus validate usage of a modified PAM_chem_v8 model to estimate concentrations of radicals in the OFR as discussed below.

Vocus PTR was applied to quantify precursor concentrations. The focusing ion-molecule reactor (FIMR) was heated up and its temperature was maintained at 100 ℃ during the experiments. The FIMR can be operated under 2.0 mbar without a strong interference from corresponding water clusters when ionizing the neutral compounds. The Vocus front and back voltages were 650 V and 15 V, respectively, forming an axial voltage of 635V and a reduced electrical field (*E/N*, where E is the electric field strength and N is the number density of the buffer gas in FIMR) of 180 Td. The radio frequency (RF) voltages and frequency were set to be 450 V and 1.3 MHz, respectively. The sample flow was introduced to the Vocus PTR through a Teflon tube with an OD of 1/4 in. and a length of 120 cm from the OFR. A total

sample flow of 1.4 slpm was maintained by a pump with an orifice to minimize the delay time of sampling, from which approximately 125 sccm was sampled into the FIMR through a capillary tube.

In the 2nd-round experiments, a Vocus CI-TOF (Towerk AG, Switzerland) equipped with a Vocus Aim inlet and the same nitrate-ion chemical ionization source as adopted in the 1st-round experiments was utilized to measure oxidation products, hereafter referred as nitrate CI-TOF. The nitrate CI-TOF was characterized with a flat transmission efficiency between m/z 60 Th and m/z 500 Th, as well as a mass resolution of 10000 at m/z 200 Th. In this series of experiments, the reaction products were sampled from the PAM OFR via a 30 cm-long Teflon tube with a 1/2 in. OD to our nitrate CI-TOF. The Vocus PTR and the ozone monitor were connected to the PAM OFR from a separate port via a 120 cm-long Teflon tube with a 1/4 in. OD.

We did not quantify HOMs' concentrations. Since the inner diameters of PAM OFR, sampling tube, and the nitrate CIMS inlet were different, and two reducing unions were used during sampling, the estimation of the penetration efficiency and sampling efficiency of HOMs are thus of a significant uncertainty. The initial concentrations of TMB utilized in both sets of experiments fluctuated slightly, which resulted from sample preparation processes and were more obvious in the 1st-round experiments. Therefore, in the discussion on the data of the 1st-round experiments, we tried to minimize potential influences of the differences in the initial TMB concentrations on the signals of HOMs by normalizing the HOMs signals with the initial TMB signal. To precisely illustrate changes in the abundance of HOMs at different OH exposures, a normalized signal was chosen to present the abundance of detected HOMs, which is defined as the ratio of the signals of HOMs in the nitrate CIMS normalized by the reagent ions and the initial signal of 1,3,5-TMB, i.e., $S(HOMs)/S(TMB)$. $S(HOMs)$ is the signal of HOM detected by the nitrate CIMS normalized with the signal of reagent ions, whereas $S(TMB)$ is the initial signal of 1,3,5-TMB detected by the Vocus PTR.

To compare chemical regimes of two series of experiments and the ambient atmosphere, a PAM chemistry model (PAM_chem_v8), utilized widely in previous studies, were chosen with the latest updates to calculate radical profiles in our OFR (Li et al., 2015; Cheng et al., 2021; Wang et al., 2020b; Mehra et al., 2020; Lambe et al., 2015, 2018; Peng and Jimenez, 2020; Lambe et al., 2017). This model is based on a photochemical box model that includes chemistry of photolysis of oxygen, water vapor, and other trace gases by the primary wavelengths of mercury lamps, and simplified VOC and RO_2 chemistry, but further reactions of the first-generation stabilized products and the second-generation organic radicals are not considered. The reactions and corresponding kinetics utilized in this model were summarized

in Table S2. In this work, autoxidation and accretion of 1,3,5-TMB-derived BPR, as well as subsequent reactions of the autoxidation product of BPR, i.e., $C_9H_{13}O_7\cdot$, are newly implemented or modified in this model (Reaction No. 46 – 62 in Table S2). These two radicals were the most significant RO_2 in the system and represented the whole RO_2 pool in the PAM chemistry model simulation. The pathways of peroxy radicals and their kinetics are discussed below. NO_x-related reactions are also included in the model. When experiments without NO_x are simulated, these NO_x-related reactions do not contribute to the simulation results.

The detailed reactions involved with RO_2 include:

$$RO_2 + R'O_2 \rightarrow RO + R'O + O_2 \quad (R1)$$

$$RO_2 + R'O_2 \rightarrow R{=}O + R'OH + O_2 \quad (R2)$$

$$RO_2 + R'O_2 \rightarrow ROH + R'{=}O + O_2 \quad (R3)$$

$$RO_2 + R'O_2 \rightarrow ROOR' + O_2 \quad (R4)$$

$$RO_2 + HO_2 \rightarrow ROOH + O_2 \quad (R5)$$

$$RO_2 + OH \rightarrow Products \quad (R6)$$

$$RO_2 \xrightarrow{isomerization} Products \quad (R7)$$

$$RO_2 + NO \rightarrow RO + NO_2 \quad (R8)$$

$$RO_2 + NO \rightarrow RONO_2 \quad (R9)$$

$$RO_2 \rightarrow physical\ loss \quad (R10)$$

$R1$, $R2$, and $R3$ are reactions of RO_2 + RO_2, forming alkoxy radicals, carbonyl termination products, and hydroxyl termination products, respectively. $R4$ is the accretion reaction, forming dimers via combination of two monomeric RO_2. $R5$ is the reaction between RO_2 and HO_2, forming hydroperoxyl radicals. The reaction rate constants for RO_2 in $R1$ – $R5$ are obtained by MCM or previous investigations (e.g., Jenkin et al., 2003; Berndt et al., 2018; Peng and Jimenez, 2020). We treat $R1$ – $R3$ as a total reaction with a reaction rate constant of 8.8×10^{-13} molecule^{-1} cm^3 s^{-1}, and branching ratios of $R1 - R3$ of 0.6, 0.2, and 0.2, respectively, as suggested by MCM (Jenkin et al., 2003). The reaction rate constants of BPR and $C_9H_{13}O_7\cdot$ for $R4$ are 1.7×10^{-10} and 2.6×10^{-10} molecule^{-1} cm^3 s^{-1}, respectively (Berndt et al., 2018b). The reaction rate constants for $R5$ is 1.5×10^{-11} molecule^{-1} cm^3 s^{-1} (Jenkin et al., 2003).

$R6$ is the reaction between OH and RO_2, whose reaction rate constant is 1×10^{-10} molecule^{-1} cm^3 s^{-1} according to previous studies (Bossolasco et al., 2014; Yan et al., 2016; Assaf et al., 2016, 2017; Peng and Jimenez, 2020). Current knowledge on the reaction products for the reaction of $CH_3O_2\cdot$ + OH, the most studied RO_2 + OH reaction, is summarized in Table S3. The products of this reaction are suggested to include a Criegee intermediate ($CH_2O_2\cdot$), a stabilized methylhydrotrioxide (CH_3OOOH), an alkoxy radical ($CH_3O\cdot$), and methanol (CH_3OH) (Yan et al., 2016; Fittschen, 2019; Caravan et al., 2018; Müller et al., 2016). Müller et al. (2016) and

Caravan et al. (2018) suggested that the formation of CH_2O_2· is actually infeasible, and Yan et al. (2016) estimated an upper limit branching ratio of 5% for this pathway. The branching ratios of stabilized products CH_3OH and CH_3OOOH are 6 – 7% (Caravan et al., 2018; Müller et al., 2016) and 7% (Müller et al., 2016), respectively. The most significant product of this reaction is the alkoxy radical (CH_3O·), with a branching ratio of more than 86% (Müller et al., 2016). In the absence of NO_x, CH_3OH and CH_3O· can also be formed via the traditional unimolecular reaction between CH_3O_2· and RO_2, i.e., $R1$ and $R3$. The possible role of this reaction of large RO_2, i.e., BPR and other C9-RO_2, with OH has not yet been investigated. However, according to the branching ratios for the reaction of CH_3O_2· + OH, this reaction is likely to form RO instead of stabilized C9 products. Hence, we assume that the branching ratios of hydrotrioxide (ROOOH), RO, and ROH are 0.07, 0.86, and 0.07, respectively, for BPR + OH and C9-RO_2 + OH.

$R7$ is the unimolecular reactions of RO_2 in the PAM OFR. RO_2 isomerization rate coefficients are highly dependent on their structures, spanning from 10^{-3} – 10^6 s^{-1} (Bianchi et al., 2019; Crounse et al., 2013; Knap and Jørgensen, 2017; Praske et al., 2018). However, only some substituted acyl RO_2 can undergo rapid isomerization at a reaction rate of 10^6 s^{-1} (Knap and Jørgensen, 2017). 1,3,5-TMB-derived BPR and its autoxidation product, $C_9H_{13}O_7$·, do not belong to this group of substituted acyl RO_2 (Molteni et al., 2018; Tsiligiannis et al., 2019). The most important unimolecular reactions for 1,3,5-TMB-derived BPR is likely autoxidation while the precise autoxidation reaction rates of 1,3,5-TMB-derived BPR and other RO_2 in this system are currently unclear (Bianchi et al., 2019; Molteni et al., 2018). Previous theoretical investigations suggest that more than 90% BPR generated by the oxidation of 1,3,5-TMB possess a structure favoring autoxidation and thus their overall autoxidation reaction rate is relatively fast (Wang et al., 2017). We follow quantum calculation results on the autoxidation reaction of a methyl group adjacent to the RO_2 functionality group (Wang et al. 2017), and time the suggested rate (0.026 s^{-1}) by 3 due to the symmetry with three methyl groups in our parent compound. The obtained autoxidation reaction rate is 0.078 s^{-1}.

$R8$ and $R9$ are the reactions between NO and RO_2, generating alkoxy radicals and organonitrates, respectively. The reaction rate for the sum of these two reactions is 8.5×10^{-12} $molecule^{-1}$ cm^3 s^{-1}. The branching ratios of these two reactions are 0.843 and 0.157, respectively, according to MCM (Jenkin et al., 2003).

Alkoxy radicals, RO, will be generated in $R1$, $R6$, and $R8$. The widely used near-explicit mechanism, MCM, assumes that RO formed via the alkoxy channel of BPR ($R1$) will decompose into small molecules. Recently, Xu et al. (2020) probed the chemical fates of BPR-derived RO, hereafter referred to as bicyclic alkoxy radical (BCP-oxy), in the oxidation of

benzene by laboratory experiments and model calculations, which can be taken as a reference to induce the mechanism of 135-TMB-derived BCP-oxy. BCP-oxy can undergo two reactions, i.e., ring-breakage and ring-closure, and a new calculation result suggests that the branching ratio of ring-breakage reaction is larger than 98% (Wang et al., 2013). 56% of ring-breakage reactions will break benzene-derived BCP-oxy into butenedial and glyoxal, and the rest 44% will generate a C6 alkyl radical by a 1,5-aldehydic H-shift. The latter C6 alkyl radical will further undergo other reactions, including a 93% branching ratio for decomposition reactions that results in a reduction of carbon atom number (Xu et al., 2020). Therefore, most of benzene-derived BCP-oxy will likely decompose into compounds with fewer carbon atoms. We assume that 1,3,5-TMB-derived BCP-oxy will undertake these decomposition reactions with a similar branching ratio, which means that these radicals cannot form a large number of stabilized products that can influence the distributions of stabilized C9 products in nitrate CIMS.

$R10$ is the physical loss of RO_2. The physical loss of RO_2 in the PAM OFR consists of the condensation loss to the aerosol particles and the diffusion loss to the OFR walls. In our experiments, measurement results by a long-SMPS show that the aerosol particles presented in the PAM OFR were few. The long SMPS consisted of a long-DMA (TSI model 3081) and a CPC (TSI model 3787), covering a particle number size distribution from 13.6 nm to 736.5 nm. Thus, though not detected in this study, we cannot absolutely deny the possibility that particles might have been generated, resulting in a larger physical loss of HOMs. This part of physical loss might be underestimated. The first-order loss rate of HOMs to the OFR walls, k_{wall}, is limited by eddy diffusion and can be calculated with the following function (Cheng et al., 2021; Palm et al., 2016; McMurry and Grosjean, 1985):

$$k_{wall} = \frac{A}{V} \cdot \frac{2}{\pi} \cdot \sqrt{k_e D_g} \qquad (Eq1)$$

where the OFR surface-area-volume ratio (A/V) is 25 m^{-1} and the coefficient of eddy diffusion (k_e) is 0.0042 s^{-1}, as estimated by the method utilized in a previous study (Brune, 2019) and given in $Eq2$.

$$k_e = 0.004 + 10^{-2.25} V^{0.74} \qquad (Eq2)$$

where V is the enclosure volume (m^3). The molecular diffusion coefficient, D_g, is estimated with the method as described by Fuller et al. (1966) and is around 5×10^{-6} m^2 s^{-1} with 1,3,5-TMB derived BPR as an example. Hence, k_{wall} is around 0.0023 s^{-1} in the PAM OFR.

Other kinetic data in the modified PAM_chem_v8 model are obtained from the IUPAC (International Union of Pure and Applied Chemistry) dataset (https://iupac-aeris.ipsl.fr, last access: 26 October 2023) and the MCM dataset (MCM v3.3.1, https://mcm.york.ac.uk/MCM/, last access: 9 October 2023).

For the 1st-round experiments, the input parameters of temperature, mean residence time, water vapor concentration, O_3 concentration, and the initial 1,3,5-TMB concentration are 25 ℃, 53 s, 0.63%, 1.23×10^{13} molecule cm^{-3}, and 1.23×10^{12} molecule cm^{-3}, respectively, as measured directly. For the 2nd-round experiments, the input parameters of O_3 concentration and the initial 1,3,5-TMB concentration were updated as 3.68×10^{12} molecule cm^{-3} and 7.55×10^{11} molecule cm^{-3}, respectively. In the NO_x experiments, the input flow rate of N_2O is 350 sccm in the 1st-round experiments and 2.5 slpm in the 2nd-round experiments, respectively. The actinic flux at 254 nm, I_{254}, is constrained by comparing OH exposures by model output and OH exposures estimated by the consumption of 1,3,5-TMB as measured by the Vocus PTR. Consumption of O_3 estimated by the model agrees well with the measured results, with discrepancies being always within 10% at different OH exposures.

3 Results and discussion

3.1 Comparison of chemical regimes

Concentration profiles of OH, RO_2, and HO_2 as a function of OH exposures in our high [OH] experiments without NO_x, i.e., the 1st-round experiments, are illustrated in Figure S1a. According to the modified PAM_chem_v8 model, when [OH] increased from 9.32×10^7 to 1.03×10^9 molecule cm^{-3}, [HO_2] increased from 7.25×10^8 to 2.79×10^9 molecule cm^{-3}, whereas [RO_2] concentrations increased from 5.17×10^9 to 9.5×10^9 molecule cm^{-3}. The radical concentrations in high [OH] experiments with NO_x (Figure S1b) varied in a similar range, with [RO_2] ranging from 4.38×10^9 to 9.13×10^9 molecule cm^{-3}, HO_2 ranging from 4.47×10^9 to 6.47×10^9 molecule cm^{-3}, and OH ranging from 3.86×10^8 to 7.82×10^8 molecule cm^{-3}, respectively. The ratios of between HO_2/OH and RO_2/OH in the 1st-round experiments were generally in the same order of magnitude as those in with the ambient atmosphere (Whalley et al., 2021).

Radical concentrations were also estimated by the PAM_chem_v8 model to illustrate the chemical regimes in the 2nd-round experiments (Table S4). The average [HO_2], [OH], and [RO_2] were 9.7×10^7, 1.64×10^7, and 1.69×10^9 molecule cm^{-3}, respectively, in Exp. 2-3, and were 6.7×10^7, 1.04×10^7, and 1.34×10^9 molecule cm^{-3}, respectively, in Exp. 2-4, both of which generally differ by no more than a factor of 3 from the summer daytime ambient ones in polluted atmospheres (Tan et al., 2017, 2018, 2019; Whalley et al., 2021; Lu et al., 2012). The average [HO_2], [OH], and [RO_2], as well as the NO and NO_2 concentrations in Exp. 2-7 are generally very close to those in the same environment (Tan et al., 2019).

We take Exp. 1-12 ([OH] = ~8.47×10^8 molecule cm^{-3} and NO_x = 0) and Exp. 2-3 ([OH] = ~1.64×10^7 molecule cm^{-3} and NO_x = 0) as representative examples and compare simulation

results with those from the ambient atmosphere, since NO_x in the ambient is believed not to impact relative ratios for $R1 - R3$, $R5$, and $R6$. In the ambient atmosphere, the average [HO_2], [OH], and [RO_2] were 2.7×10^8, 8.0×10^6, and 1.4×10^9 molecule cm^{-3}, respectively, around summertime noon in urban Beijing (Whalley et al. 2021), and $(4 - 28)\times10^8$, $(0.8 - 2.4)\times10^7$, and 1.2×10^9 molecule cm^{-3} (modeled) at a suburban site in Yangtze River Delta (Ma et al. 2022). As shown in Figure 1a, for the most important RO_2, BPR, the fractions of monomeric termination reactions of RO_2 + RO_2 ($R1 - R3$), RO_2 + HO_2 ($R5$), and RO_2 + OH ($R6$) were 6.2%, 29.3%, and 64.5%, respectively, in Exp.1-12. In contrast, the fractions were 32.5%, 31.8%, and 35.7%, respectively, in Exp. 2-3, whereas the values were 20.3%, 66.6%, and 13.2%, respectively, for summertime, urban Beijing.

(a)

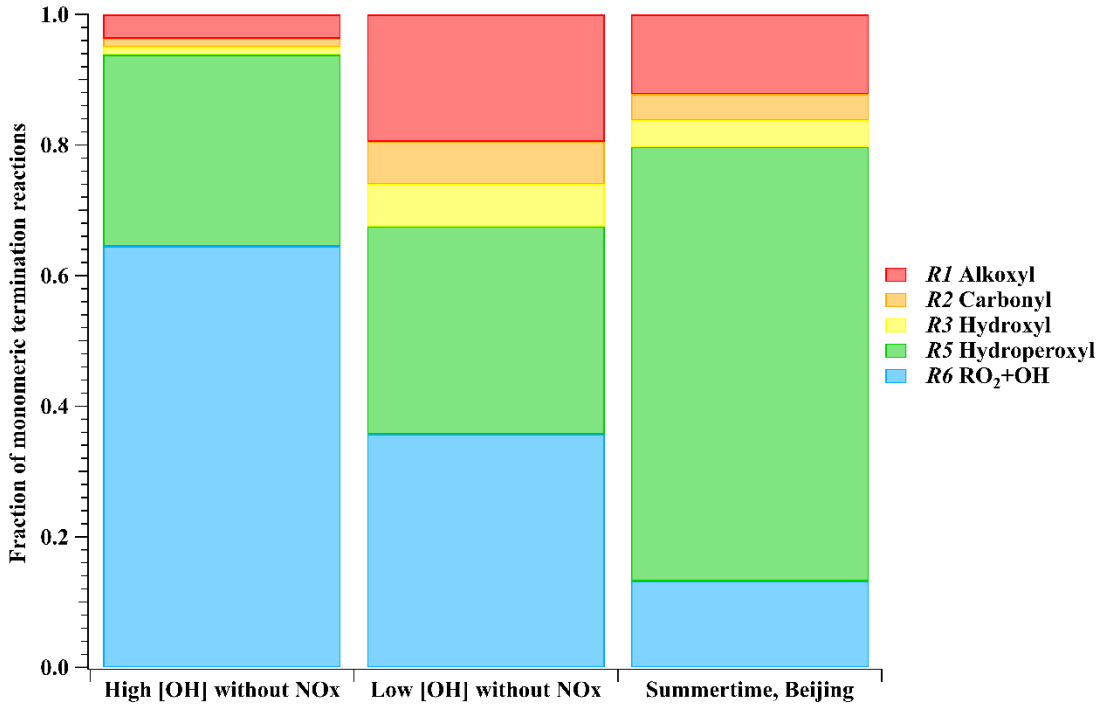

429 **(b)**

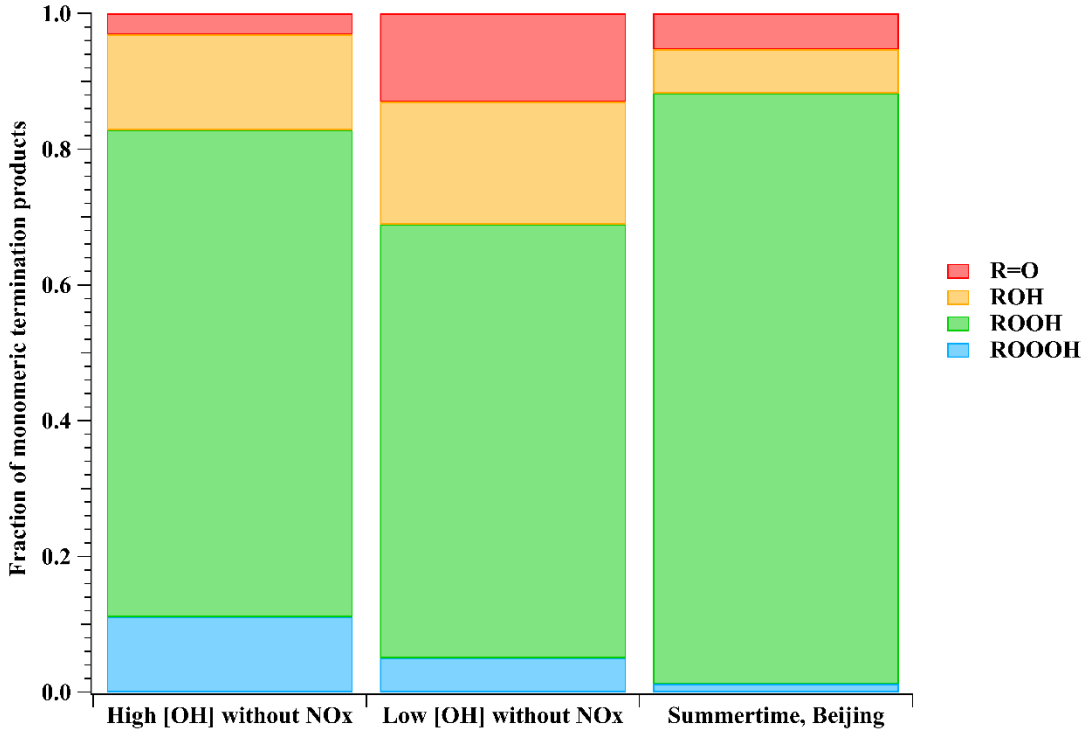

430

431 **(c)**

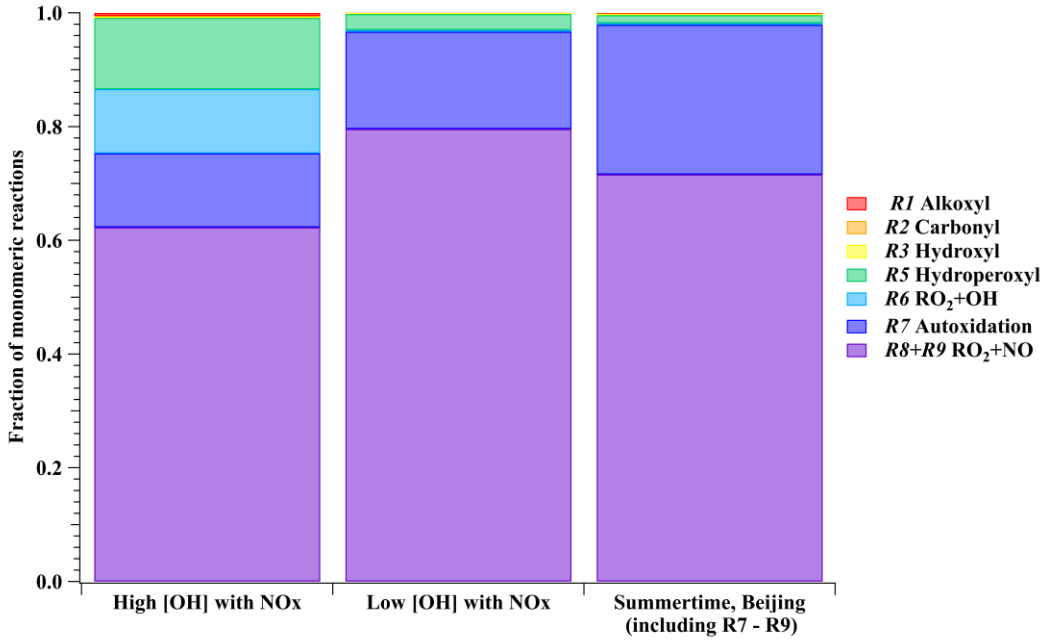

432

(d)

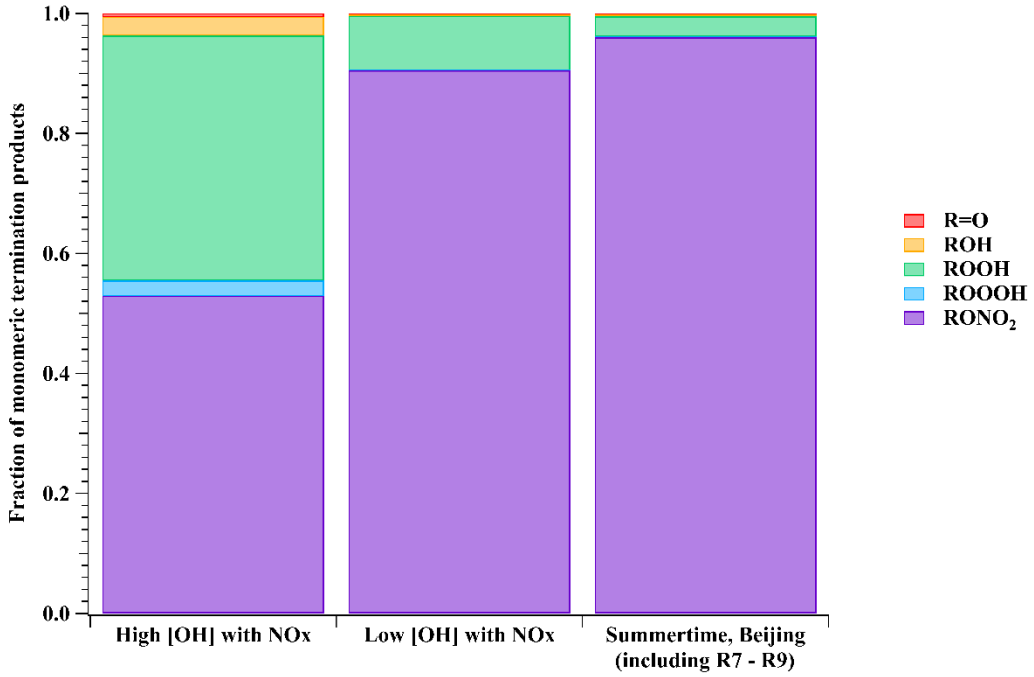

Figure 1. (a) The fraction of monomeric termination reactions and (b) monomeric termination products of BPR in a representative high [OH] experiment without NO_x (Exp. 1-12), a representative low [OH] experiment without NO_x (Exp. 2-3), and summertime, urban Beijing (Whalley et al. 2021). NO_x related reactions and products for the Beijing study are not included for a better comparison. (c) The fraction of monomeric reactions (R1 – R3 and R5 – R9) and (d) monomeric termination products of BPR in a representative high [OH] experiment with NO_x (Exp. 1-48), a representative low [OH] experiment with NO_x (Exp. 2-7), and summertime, urban Beijing (Whalley et al. 2021). Reactions and kinetic rate coefficients used in the calculations are provided in Table S2.

Our NO_x-free experiments are characterized with an inherent drawback that the proportion of the HO_2 termination pathway ($R5$) is actually lower than that under ambient conditions, which is similar to most other laboratory experiments (Bianchi et al., 2019). In our high [OH] experiments without NO_x, the reaction rates of unimolecular reactions, e.g., autoxidation reaction ($R7$) and condensation ($R10$) did not change with [OH] that increased in our experiments relative to that in the ambient. As a result, relative proportions of autoxidation and condensation were lowered. On the other hand, 1,3,5-TMB-derived BPR was suggested to undergo autoxidation ($R7$) at a reaction rate of 0.078 s^{-1} (Wang et al., 2017), which represented 36.8%, 94.4%, and 92.8% of the overall rates of $R1$ – $R3$ and $R5$ – $R7$ in Exp. 1-12, Exp. 2-3, and summertime, urban Beijing, respectively. Because of its dominant proportion in Exp. 2-3 and the ambient, the autoxidation channel is not included for clarity in Figure 1a. Autoxidation

did possess a lower significance in our high [OH] experiments due to the other accelerated bimolecular reactions. However, it would only influence the oxygen content of our products but would not change the DBE. Both accretion reaction ($R4$) and condensation ($R10$) have been taken into account in the model, but they would not influence the distributions of monomeric stabilized products. We will specifically discuss these two pathways in the following sections because of their complexity between the laboratory and ambient conditions.

RO_2 other than BPR and $C_9H_{13}O_7^{\cdot}$ existed in the PAM OFR, which were not included in the model simulation. Their reaction rates of the accretion reaction ($R4$) and the autoxidation reaction ($R7$) should be different from BPR and $C_9H_{13}O_7^{\cdot}$ due to the strong dependence of these two reaction rates on the molecular structure. Rates for the other reaction channels, on the other hand, should be the same as those of BPR and $C_9H_{13}O_7^{\cdot}$. Therefore, their fates in terms of the monomeric termination reactions ($R1 - R3$, $R5 - R6$, and $R8 - R9$) should be similar as BPR and $C_9H_{13}O_7^{\cdot}$.

Calculated from yields of stabilized monomeric termination products of BPR, the fractions of monomeric termination reaction products in Exp. 1-12, Exp. 2-3, and summertime, urban Beijing (Whalley et al. 2021) are presented in Figure 1b, showing a lot of similarities between these conditions. The fractions of R=O, ROH, ROOH, and ROOOH in Exp. 1-12 were 3.1%, 14.1%, 71.7%, and 11.1%, respectively. These fractions were 13.0%, 18.1%, 63.9%, and 5.0%, respectively, in the Exp. 2-3, and were 5.3%, 6.5%, 87.0%, and 1.2%, respectively, in the summertime Beijing case. Among them, the majority of products are always ROOH and ROH, with ROOH being the most abundant. Therefore, the monomeric termination products of BPR in our experiments are atmospheric relevant. In addition, only the R=O product has a DBE higher than the reacted RO_2, but merely accounted for a limited proportion. All the other stabilized termination products have a DBE that is 1 lower than the precursor, and are the majority in both laboratory and ambient conditions. This indicates that the majority of the first-generation products typically have a DBE that is 1 lower than that of 1,3,5-TMB, whereas the majority of subsequent-generation products typically have a DBE that is 2 lower than that of 1,3,5-TMB. Once a monomeric compound with a DBE that is at least 2 lower than that of 1,3,5-TMB was observed, multi-generation OH reactions have happened in the system.

In laboratory experiments in absence of NO_x (e.g., Exp.1-12), the proportions of $R8 - R9$, i.e., the NO channel in the urban atmosphere were attributed to termination reactions of $R1 - R6$, i.e., $RO_2 + RO_2$, accretion reaction, $RO_2 + HO_2$, and $RO_2 + OH$. By expanding proportions of these termination reactions, laboratory investigations on product distributions can be facilitated, as the detection of certain HOM products became more precise and the mass spectra became simplified.

In experiments with NO_x, the chemical fates of BPR in high [OH] experiments (Exp. 1-48 as an example, [OH] = ~6.77×10^8 molecule cm^{-3}, NO = ~4.73×10^{10} molecule cm^{-3}. NO_2 = ~1.67×10^{12} molecule cm^{-3}), low [OH] experiments (Exp. 2-7 as an example, [OH] = ~1.69×10^7 molecule cm^{-3}, NO = ~3.19×10^{10} molecule cm^{-3}. NO_2 = ~2.70×10^{11} molecule cm^{-3}), and the summertime, urban Beijing are compared. As shown in Figure 1c, in all three conditions, RO_2 reactions with NO were always the most significant pathway, with autoxidation being the second most significant.

Accounting for at least 52% of monomeric termination products under all conditions, organonitrates were always the most important termination products, as shown in Figure 1d. On the other hand, based on the formulae of organonitrates, the detailed formulae of monomer RO_2 could be probed, which can help us better understand the chemical reactions inside the system. Alkoxy radicals generated in the NO termination channel will unlikely influence the distributions of C9 stabilized products since they tend to get decomposed in the subsequent reactions, as discussed in our previous discussion on the fate of alkoxy radicals in Section 2.

Due to the complexity of ambient RO_2 pool, it is difficult to estimate the detailed fraction of accretion reactions $R4$. In the laboratory experiments, RO_2 pool mainly consists of BPR and its autoxidation reaction product $C_9H_{13}O_7\cdot$, which both can undergo accretion reaction rapidly (Berndt et al., 2018b). The concentrations of these two radicals were estimated by PAM_chem_v8. The reaction rate of accretion ($R4$) for BPR was around 1.61 s^{-1} in Exp.1-12, being 88.4% of $R1-R7$, and was 0.29 s^{-1} in Exp.2-3, equivalent to 77.7% of $R1-R7$. Certain uncertainties exist in the estimation of the proportions of accretion reactions, as the PAM_chem_v8 model only includes the first-generation reactions of precursors, whereas the subsequential fragmentation and re-initiation of stabilized products can generate a series of new RO_2 that will influence the proportions of accretion reactions. We are only certain that the significance of accretion reactions in both Exp. 1-12 and Exp. 2-3 is larger than the ambient. The much-expanded proportion of HOM dimers through accretion reactions makes it inadequate to compare yields of HOM dimers and HOM monomers. However, this deviation will not influence our conclusion on multi-generation OH oxidation and identification of HOM dimers can help us identify the exact RO_2 in the OFR and confirm the conditions of secondary OH oxidation according to the number of hydrogen atoms in the molecules.

In addition, certain compounds might have condensed onto pre-existing particles in the real atmosphere before an appreciable fraction of such compounds undergoes the re-initiated OH oxidation. Therefore, even if the same product can be generated both in the laboratory experiments and the ambient atmosphere, the relative significance of this product is not completely identical. Though OOMs might have the potential to undergo multi-generation OH

oxidation, the exact proportion of this reaction in the ambient strongly depends on their volatility, in other words, condensation sink of these OOMs. The typical monomeric termination products of 1,3,5-TMB-derived BPR, $C_9H_{12}O_4$, $C_9H_{14}O_4$, $C_9H_{14}O_5$, and $C_9H_{13}NO_6$, are estimated to have saturation vapor concentrations (C*) of 30.20, 30.20, 0.85, and 3.39 μg/m^3 at 300 K, respectively with the volatility parameterization developed in the CLOUD chamber oxidation experiments of aromatics (Wang et al., 2020a). From the perspective of volatility, they all belong to semi-volatile organic compounds (SVOC, 0.3 < C* < 300 μg/m^3) and are expected to exist in both the condensed and the gas phases at equilibrium in the atmosphere (Bianchi et al., 2019). Compared to ambient conditions, the proportion of their condensation in the laboratory were biased to be lower due to the accelerated bimolecular reactions. However, this will not prevent the high [OH] experiments from showing the potential and ability of these compounds to go through re-initiated OH oxidation, as these compounds would exist in significant fractions in the gas phase in the real atmosphere.

However, the conditions are completely different for other HOM monomer products and HOM dimer products with much lower volatility. It is difficult for a HOM dimer, e.g., $C_{18}H_{26}O_{10}$ estimated with a C* of 7.24×10^{-13} μg/m^3 at 300 K, to survive long enough to experience an appreciable re-initiated photochemical ageing. The lifetime of HOMs that can be classified as LVOCs (3×10^{-5} < C* < 0.3 μg/m^3) and ELVOCs (C* < 3×10^{-5} μg/m^3) can be estimated according to the condensation sink (CS) in the atmosphere, as they are lost irreversibly onto surfaces. The median value of CS in urban Beijing was reported to be around 0.019 s^{-1} and 0.057 s^{-1} during NPF days and non-NPF days, respectively, whereas the values in Shanghai were reported to be around 0.013 s^{-1} and 0.017 s^{-1}. respectively (Deng et al., 2020; Yao et al., 2018), which are all much higher than the physical loss in our PAM OFR, i.e., 0.0023 s^{-1}. LVOCs and ELVOCs are believed to be lost irreversibly to the surface in both the laboratory and ambient because of their low volatility. By assuming a similar diffusion coefficient of LVOCs and ELVOCs to that of sulfuric acid, the lifetimes of LVOCs and ELVOCs in the ambient still can still be as high as 77 s for the condensation loss, which is close to the residence time of our PAM OFR. Therefore, if they were generated by oxidation of aromatics in the ambient, these LVOCs and ELVOCs should at least have the potential to experience the same OH exposures as those in our low [OH] experiments, i.e., at least 5.86×10^8 molecule cm^{-3} s. On the other hand, the detailed proportions of LVOCs and ELVOCs after a large OH exposure should be lower than those in the lab due to their magnified physical loss in the ambient. This means that if the multi-generation products of those compounds were observed in the ambient air, they should have been generated via a reaction that happened very recently.

3.2 Oxidation products in high [OH] experiments

A total of 33 HOM monomers with formulae of $C_{7\text{-}9}H_{8\text{-}16}O_{6\text{-}11}$ and 22 HOM dimers with formulae of $C_{17\text{-}18}H_{24\text{-}30}O_{8\text{-}14}$ were observed in the 1st-round experiments of gas phase OH-initiated oxidation of 1,3,5-TMB in the OFR, i.e., high [OH] experiments, as listed in Table S5. The relative signal contributions of HOMs to the total signals of all HOMs at an OH exposure of 2.38×10^{10} molecules cm^{-3} s are listed as an example in Table S5. The most abundant HOM products were also shown in stack in Figure 2, whose relationships with OH exposures are superimposed by a gamma function ($f(x) = ax^m e^{-x}$) simulation line to guide the eyes. The sum of normalized HOM monomers' abundance increased monotonically up to the highest OH exposure of 5×10^{10} molecule cm^{-3} s, whereas those of HOM dimers showed a non-monotonic dependence on OH exposure. The observed faster increase of accretion products than that of HOM monomers can be explained jointly by the fast second-order kinetics for accretion reactions of RO_2 (Berndt et al., 2018b) and the high concentrations of relevant radicals in this work. On the other hand, most of the first-generation HOM dimers formed from accretion reactions contain at least one C=C bond and have more functionalities than HOM monomers, and thus should be more reactive to OH radicals, which, together with a faster deposition loss of dimers, results in a faster consumption of HOM dimers than monomers in the OFR. The faster production and consumption of HOM dimers allowed their concentrations to summit at middle levels of OH exposures. As stated in Section 3.1, because of the inherent disadvantage of laboratory experiments, [RO_2] is always too high in the OFR, which has been pointed out in a previous study (Bianchi et al., 2019). The accretion reactions in the OFR are relatively more significant than it should be in the ambient atmosphere. We do not mean to compare the abundance of HOM monomer and HOM dimer crossly here, but to pay attention to the molecular characterization.

583 **(a)**

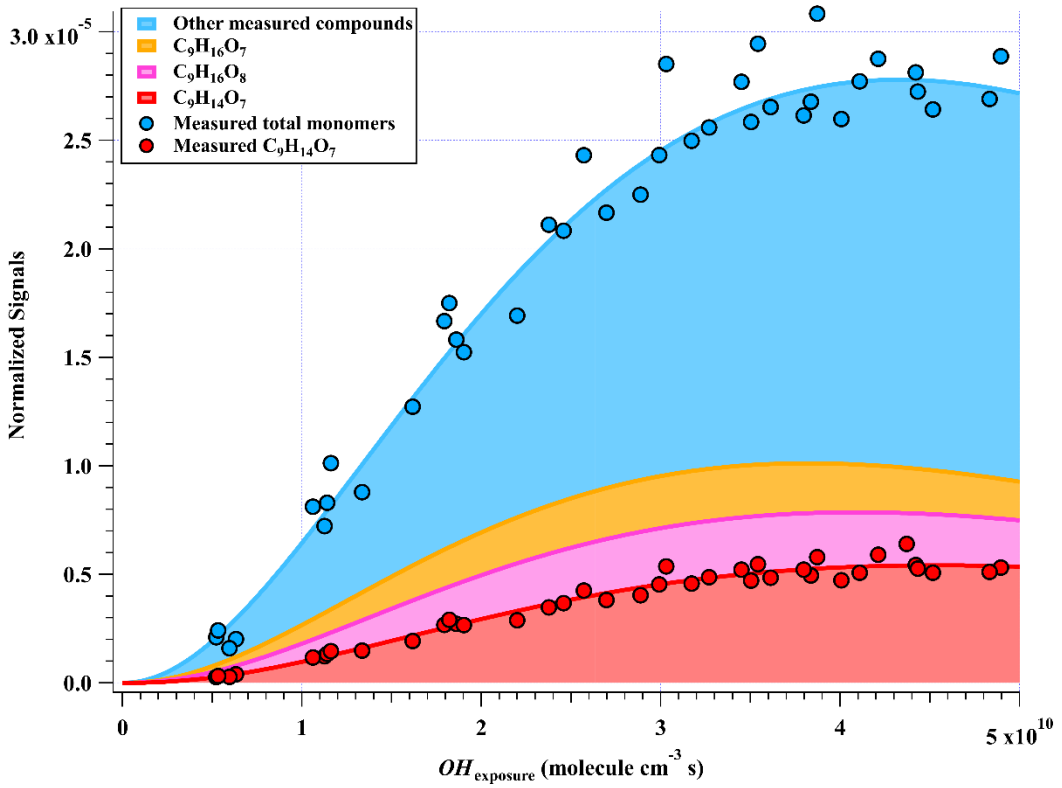

584

585 **(b)**

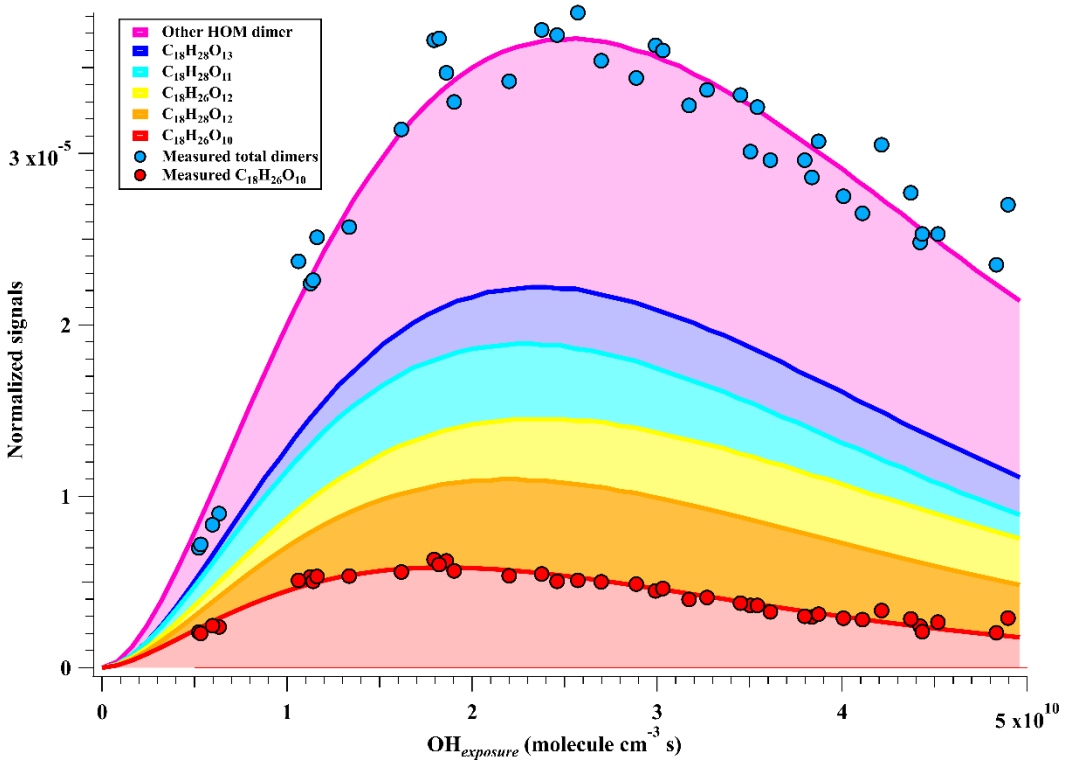

586

587 **Figure 2.** Normalized signals of (a) HOM monomers and (b) HOM dimers versus OH exposure
588 in the high [OH] experiments, which are fitted via a gamma function and shown in stack.

Theoretically, at a given RH and UV (i.e., a given [OH]), an increase in the initial TMB would lead to formation of more RO_2, which corresponds to a larger RO_2/OH. However, under our high [OH] experimental conditions, the RO_2/OH/HO_2 channels of RO_2 radicals are always minor, and thus an increase in RO_2/OH would not have a significant impact on the relative distribution of products formed from these channels. We compared product MS for experiments with a similar OH exposure but different initial concentrations of TMB (e.g., Exp. 1-3 v.s. Exp. 1-19, and Exp. 1-12 v.s. Exp. 1-22). The OH exposures of Exp. 1-3 and Exp. 1-19 were estimated by the consumption of precursors to be 5.2×10^9 and 5.3×10^9 molecule cm^{-3} s, respectively, but the initial concentration of TMB of Exp. 1-3 was 25% more than that in Exp. 1-19. Meanwhile, the OH exposures of Exp. 1-12 and Exp. 1-22 were 4.5×10^{10} and 4.4×10^{10} molecule cm^{-3} s, respectively, but the initial concentration of TMB of Exp. 1-12 was 48% more than that in Exp. 1-22. Figure S2 shows comparisons between the product MS of Exp. 1-3 and Exp. 1-19, as well as of Exp. 1-12 and Exp. 1-22, indicating that increase in the initial concentration of precursors generally resulted in a minor increment in the absolute signals of HOMs. Clearly, the relative distributions of products in these experiments are quite similar, indicating a minor difference in the relative distributions of products caused by fluctuations of initial concentrations of TMB.

3.2.1 HOM monomers

Previous studies indicate that oxidation products derived from the peroxide-bicyclic pathway represent a main fraction of HOMs (Wang et al., 2017; Zaytsev et al., 2019). For 1,3,5-TMB, this pathway, as recommended by MCM, starts from a BPR, $C_9H_{13}O_5$· (MCM name: TM135BPRO2) (Molteni et al., 2018). According to MCM and Molteni et al. (2018), Scheme 1 has been proposed to provide a good understanding of this reaction system and the structures of oxidation products. Molteni et al. (2018) suggested that $C_9H_{13}O_7$·, i.e., peroxy radical formed from autooxidation of $C_9H_{13}O_5$· has two isomers. A second-step of endo-cyclization is required in the formation of one of the isomer, which is extremely slow and not competitive as shown in several previous studies using both experimental and theoretical approaches (Wang et al., 2017; Xu et al., 2020). Even if such a second O_2 bridging to a double bond is assumed to be possible, the abundance of this isomer should be significantly smaller than the other one, because of the much faster reaction rate of H-shift reaction. Therefore, we do not take the $C_9H_{13}O_7$· isomer containing a double endo-cyclization into consideration in this work. The majority of HOM monomers is generated from subsequent reactions of $C_9H_{13}O_5$· and newly formed $C_9H_{13}O_7$·, both of which contain one C=C bond in the carbon backbone and thus have a feasible site for OH addition. Meanwhile, the autoxidation reaction rate for newly formed $C_9H_{13}O_7$· should be significantly smaller than $C_9H_{13}O_5$·, as there is no hydrogen atom in

$C_9H_{13}O_7$· that is able to undergo a hydrogen atom shift at an appreciable rate based on our current understanding. Therefore, the subsequent autoxidation reaction should not be able to generate large amounts of more oxidized RO_2.

Monomeric termination products of BPR, as shown in Scheme 1, were not detected by nitrate CIMS in this round of experiments, which might be due to the fast sub-sequential OH oxidation of these products under high [OH] environment since they were observed under low [OH] environments as shown in Section 3.3. Monomeric termination products of $C_9H_{13}O_7$· were all observed clearly, including $C_9H_{12}O_6$, $C_9H_{14}O_6$, and $C_9H_{14}O_7$. Especially, $C_9H_{14}O_7$ was the most abundant one among all of the HOM monomer products (Figure 2a). As proved by a previous study, these three species should be typical first-generation stabilized products derived from autoxidation (Wang et al., 2020b). These HOM monomers should consist of several isomers bearing the same formula, because products from the secondary reactions cannot share the same structure as that of the one from the first-generation reaction. However, limited by the inherent disadvantages of mass spectrometers, we could not distinguish isomers here and further illustrate their different chemical behaviors.

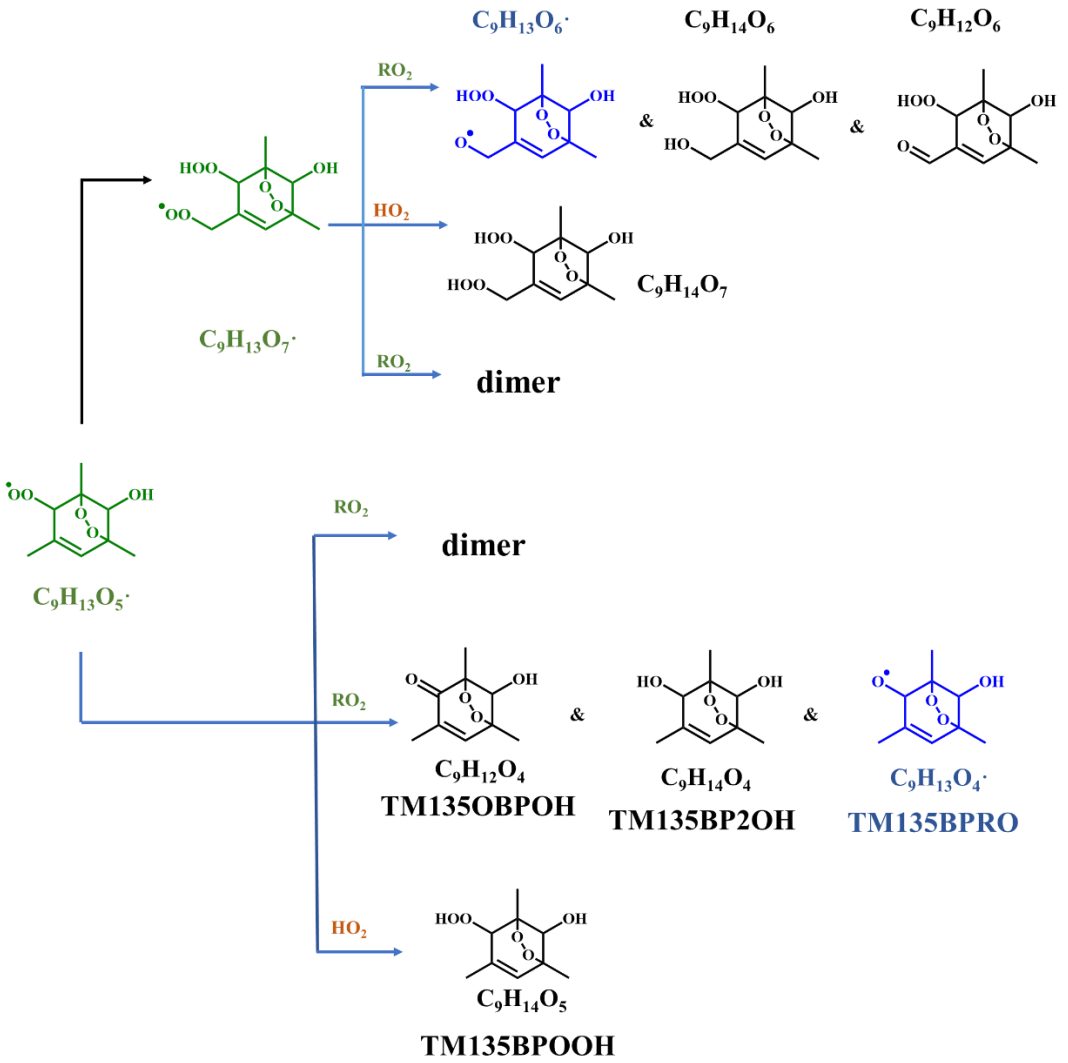

639

640 **Scheme 1.** Oxidation pathways of the bicyclic peroxy radical $C_9H_{13}O_5$· (MCM name:
641 TM135BPRO2) in the OH-initiated oxidation of 1,3,5-TMB. Green, blue, and black formulae
642 denote alkyl peroxy radicals, alkoxy radicals and stabilized products, respectively. Black
643 arrows denote the autoxidation pathway. MCM names for HO_2- and RO_2-termination products
644 of TM135BPRO2 are present.

645 In addition to these three ones, the next most prominent products to $C_9H_{14}O_7$ were $C_9H_{16}O_7$
646 and $C_9H_{16}O_8$ (Figure 3a), which are produced from multi-generation oxidation according to
647 their DBE. Based on the formulae of these three HOM monomers, they ($C_9H_{14}O_7$, $C_9H_{16}O_7$, and
648 $C_9H_{16}O_8$) could be formed from the bimolecular termination reactions of $C_9H_{15}O_8$•, which can
649 be generated by an OH attack to $C_9H_{14}O_5$ (Scheme 2), the hydroperoxyl termination product of
650 the BPR, $C_9H_{13}O_5$•. The other HOM monomers characterized with high signals were $C_9H_{14}O_8$
651 and $C_9H_{16}O_9$ (Figure 3b). These two HOM monomers ($C_9H_{14}O_8$ and $C_9H_{16}O_9$), together with
652 $C_9H_{16}O_8$, correspond to the monomeric termination products of $C_9H_{15}O_9$•, which is highly likely

the peroxy radical generated by an OH attack to $C_9H_{14}O_6$ (Scheme 3), i.e., the hydroxyl termination product of $C_9H_{13}O_7$·. As discussed earlier, $C_9H_{13}O_7$· is a typical autoxidation reaction product of the BPR of $C_9H_{13}O_5$·. Therefore, detected signals of $C_9H_{16}O_8$ should be the sum of two isomers' signals at least. Other HOM monomers were generally observed at much lower signals and thus were not plotted individually.

(a)

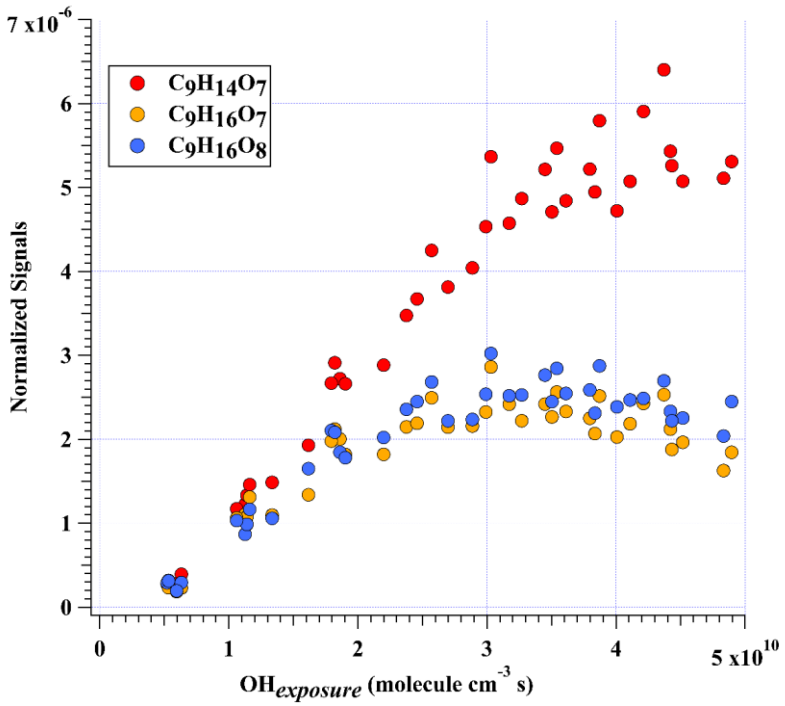

(b)

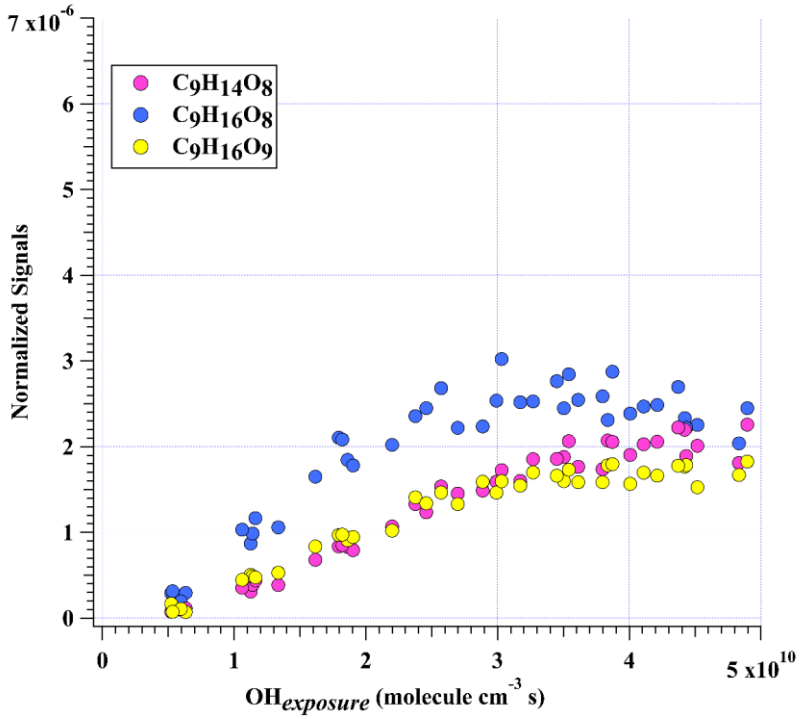

Figure 3. Normalized signals of (a) $C_9H_{14}O_7$, $C_9H_{16}O_7$, and $C_9H_{16}O_8$ and (b) $C_9H_{14}O_8$, $C_9H_{16}O_8$, and $C_9H_{16}O_9$ measured at the exit of OFR in our high [OH] experiments without NO_x as a function of OH exposure. $C_9H_{16}O_8$ are shown in both plots to better illustrate the chemical profiles of different compound groups.

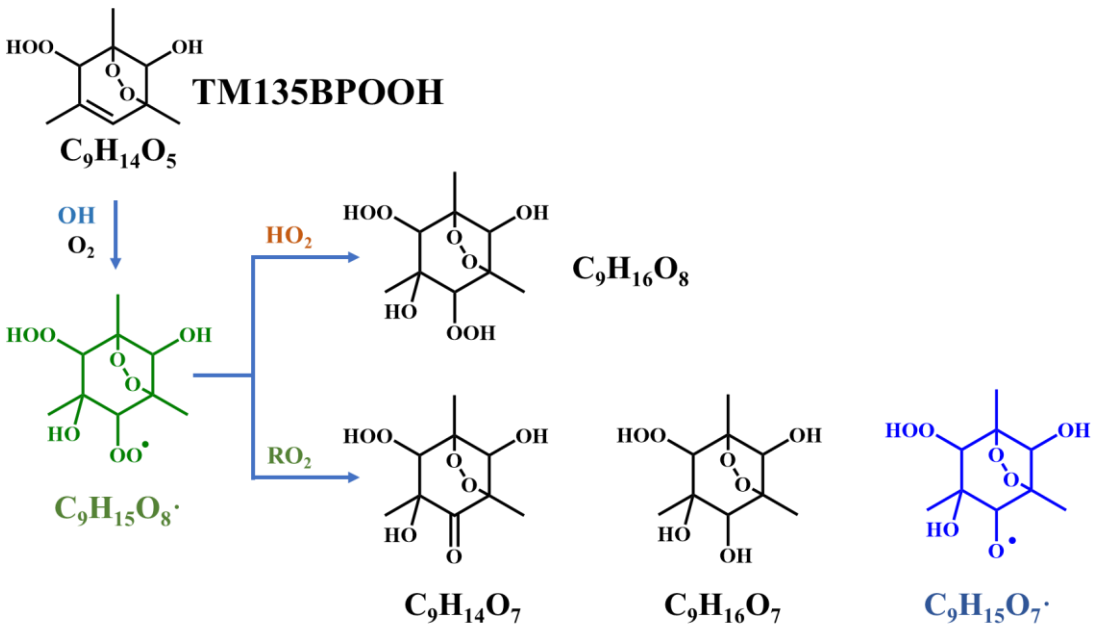

Scheme 2. Proposed formation pathways of $C_9H_{14}O_7$, $C_9H_{16}O_7$, and $C_9H_{16}O_8$ via the secondary OH oxidation of TM135BPOOH.

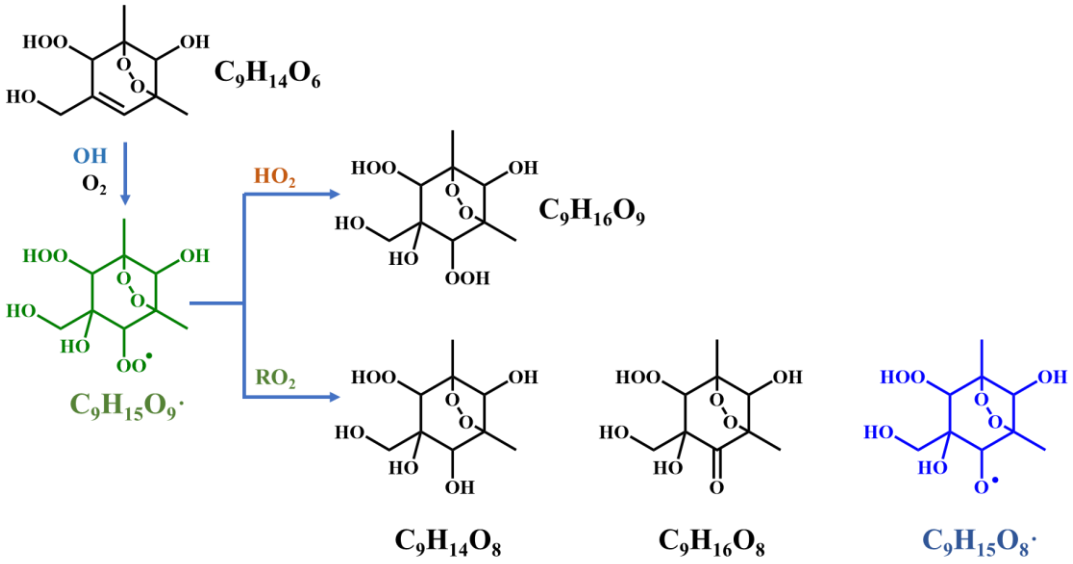

Scheme 3. Proposed formation pathways of $C_9H_{14}O_8$, $C_9H_{16}O_8$, and $C_9H_{16}O_9$ via the secondary OH oxidation of TM135BPOOH.

It is worth noting that HOM monomers with 18 hydrogen atoms, i.e., a DBE of 1, were never observed in our experiments, including a potential stabilized hydroperoxyl products formed from $C_9H_{17}O_m$·. This is expected, since $C_9H_{17}O_m$· should be in really low concentrations, if ever existed. As indicated by its hydrogen number, a $C_9H_{17}O_m$· was formed by at least two OH additions to the C=C bond of a $C_9H_{13}O_m$·, but the main BPR, $C_9H_{13}O_5$·, and its autoxidation product ($C_9H_{13}O_7$·), are characterized with one C=C bond on the ring, which makes this formation pathway impossible. Other ring-breakage pathways should not contribute to the formation of this radical ($C_9H_{17}O_m$·) because of their low branching ratio as determined by recent studies (Zaytsev et al., 2019; Xu et al., 2020).

Proposed according to MCM and Molteni et al. (2018), scheme 4 shows the NO termination pathways of the main BPR $C_9H_{13}O_5$· and its autoxidation product, $C_9H_{13}O_7$·. After introducing N_2O into PAM OFR, quantities of organonitrates were generated, including both C9 and C18 organonitrates. The averaged mass spectrometry of nitrate CIMS in the 4.41×10^{10} molecule cm^{-3} NO experiment and 1.18×10^{11} molecule cm^{-3} NO experiment is shown in Figure S3. Organonitrates were formed via the NO + RO_2 reaction, called as NO termination reactions. The distribution of oxidation products under these two NO settings were similar.

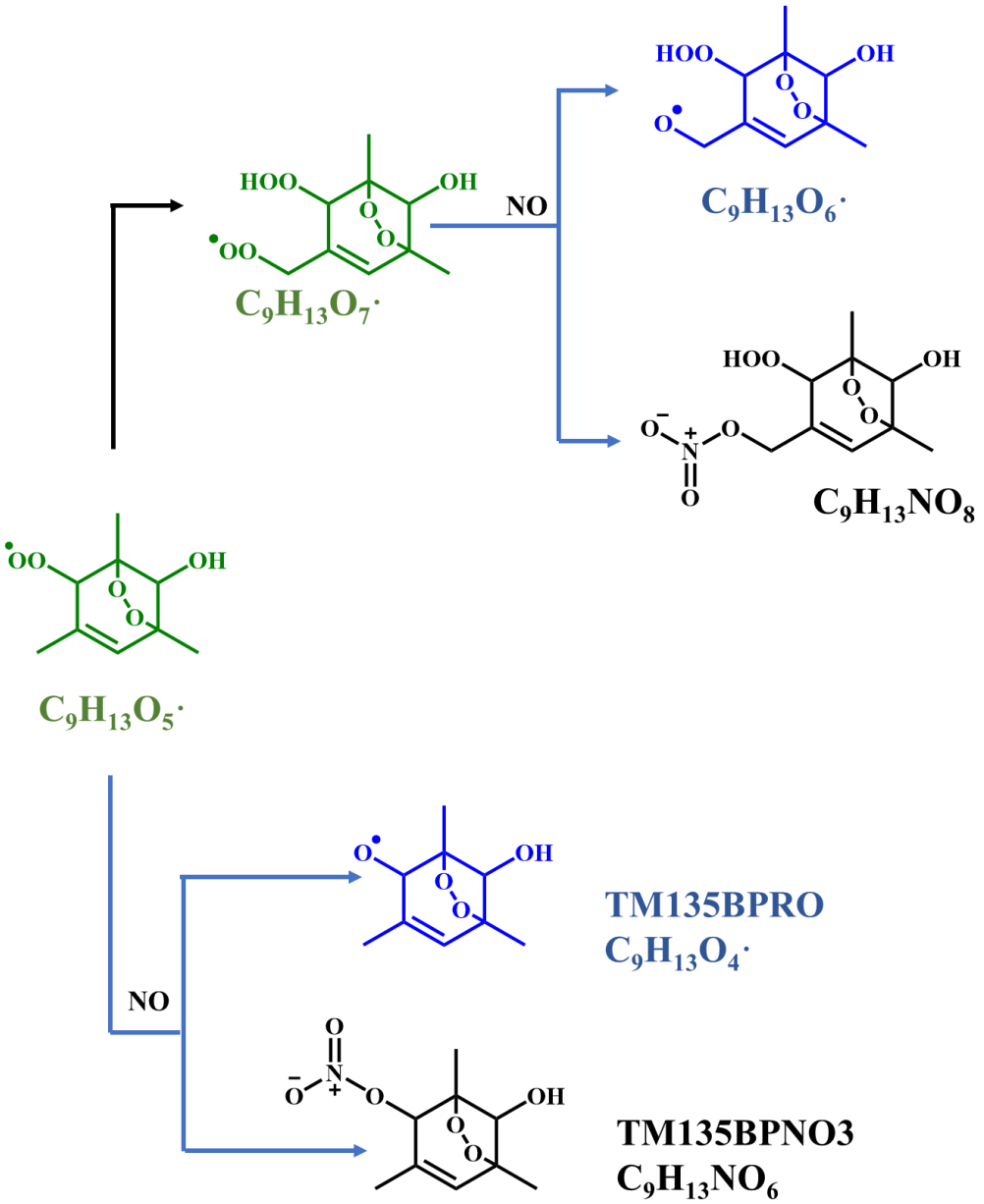

688

689 **Scheme 4**. NO termination reactions of the bicyclic peroxy radical $C_9H_{13}O_5$· (MCM name:
690 TM135BPRO2) and its autoxidation reaction products. Green, blue, and black formulae denote
691 alkyl peroxy radicals, alkoxy radicals and stabilized products, respectively. Black arrows
692 denote the autoxidation pathway. MCM names of NO-termination products of TM135BPRO2
693 are present.

694 As discussed above, most of the first-generation HOMs should contain a C=C bond in the
695 carbon backbone. The ubiquitous existence of organonitrates that contain two nitrogen atoms
696 exactly confirms the extensive secondary OH oxidation in the systems, because the NO
697 termination reaction of RO_2 is the only pathway that can generate organonitrates in our
698 experiments and this pathway can only introduce one nitrogen atom at a time, as indicated in
699 Scheme 4. RO_2 can react with NO_2 to form peroxynitrates ($ROONO_2$) but these species are

thermally unstable except at very low temperatures or when the RO_2 is an acylperoxy radical (Orlando and Tyndall, 2012), neither of which were not met in our experiments. The concentrations of NO_3 were estimated to be lower than 2.45×10^7 molecule cm^{-3} by our modified PAM_chem_v8 because of the existence of decent concentrations of NO, which would consume NO_3 at a rapid reaction rate, i.e., 2.7×10^{-11} $molecule^{-1}$ cm^3 s^{-1} (IUPAC dataset , https://iupac-aeris.ipsl.fr, last access: 26 October 2023). Therefore, NO_2 and NO_3 were not likely to react with RO_2 to form large amounts of organonitrates in our experiments. Taking the most abundant organonitrate, $C_9H_{14}N_2O_{10}$, as an example, it was exactly the NO termination product of $C_9H_{14}NO_9$·, which was generated from an OH attack and a subsequent O_2 addition to $C_9H_{13}NO_6$, the NO termination product of $C_9H_{13}O_5$·. For other organonitrates, $C_9H_{13}NO_8$, the second most abundant organonitrate, could be either a NO termination product of $C_9H_{13}O_7$· or, together with other most abundant organonitrates, $C_9H_{15}NO_7$ and $C_9H_{15}NO_8$, classical termination products of $C_9H_{14}NO_9$·. $C_9H_{14}N_2O_{10}$, $C_9H_{15}NO_7$, and $C_9H_{15}NO_8$ all have a DBE of 2 lower than the precursor and thus are the typical multi-generation OH oxidation products.

The NO:RO_2 ratio in the PAM OFR in this series of experiments is lower than typical values in the ambient atmosphere, which is due to the existence of O_3 that was utilized to generate $O(^1D)$ in the OFR and its rapid reaction rate with NO. However, due to rapid reaction rate constants between NO and RO_2, i.e., around 8.5×10^{-12} $molecule^{-1}$ cm^3 s^{-1}, the reaction rate for the NO termination channel of RO_2 was as fast as around 0.3 – 1.0 s^{-1}. Large amounts of organonitrates would still be formed, as discussed in Section 3.1. Our conclusion is also valid because of detection of compounds with multiple nitrogen atoms.

3.2.2 HOM dimers

Accretion reaction $RO_2 + RO'_2 \rightarrow ROOR' + O_2$ is a source of gas-phase dimer compounds from highly oxidized, functional RO_2 radicals (Ehn et al., 2014; Berndt et al., 2018b; Zhao et al., 2018; Berndt et al., 2018a). $C_{18}H_{26}O_8$ and $C_{18}H_{26}O_{10}$ are two typical accretion reaction products in the 1,3,5-TMB + OH system, whose formation pathways have been elucidated (Berndt et al., 2018b). $C_{18}H_{26}O_8$ can only be formed via the accretion reaction of two $C_9H_{13}O_5$·. $C_9H_{13}O_3$· is not likely to react with $C_9H_{13}O_7$· to form large amounts of $C_{18}H_{26}O_8$. $C_9H_{13}O_3$· can only be formed after addition of a hydroxyl radical to the aromatic ring of 1,3,5-TMB and a subsequent O_2 addition to the newly formed hydroxyl-substituted cyclohexadienyl radical (Vereecken, 2019). However, the lifetime of this radical is extremely short, as $C_9H_{13}O_3$· will undertake a ring-closure reaction and get attached by a O_2 very rapidly, forming BPR, $C_9H_{13}O_5$·. Its short lifetime and low concentration, as indicated by Berndt et al. (2018), lead to its insignificant role in the accretion reactions. In contrast, $C_{18}H_{26}O_{10}$ can be formed either by the accretion reaction between $C_9H_{13}O_5$· and $C_9H_{13}O_7$·or via a second OH attack to $C_{18}H_{26}O_8$.

These two HOM dimers are so far the only ones that are confirmed to be formed via the accretion reactions (Berndt et al., 2018b; Bianchi et al., 2019).

$C_{18}H_{26}O_{10}$ was characterized with the highest dimer signals for experiments with OH exposures under 3.5×10^{10} molecule cm^{-3} s. Nevertheless, $C_{18}H_{26}O_{10}$, together with $C_{18}H_{28}O_{12}$, $C_{18}H_{26}O_{12}$, $C_{18}H_{28}O_{11}$, $C_{18}H_{28}O_{13}$, and $C_{18}H_{28}O_{10}$ contributed more than 50% of total HOM dimer signals at any OH exposure levels (Figure 2b). These six most abundant HOM dimers correspond exactly to the hydroperoxyl, hydroxyl, and carbonyl termination products of $C_{18}H_{27}O_{11}$· and $C_{18}H_{27}O_{13}$·, respectively. These two RO_2 ($C_{18}H_{27}O_{11}$· and $C_{18}H_{27}O_{13}$·), on the other hand, could be generated by OH attacks to $C_{18}H_{26}O_8$ and $C_{18}H_{26}O_{10}$, respectively, which strongly suggests the significant role of secondary OH chemistry in the formation of HOMs in our experiments. In addition, $C_{18}H_{28}O_x$ can also be formed through accretion of a $C_9H_{13}O_m$· radical and a $C_9H_{15}O_m$· radical, as suggested by previous studies (Molteni et al., 2018; Tsiligiannis et al., 2019). However, since a $C_9H_{15}O_m$· radical, as suggested by its hydrogen atom number, can only be formed via an OH addition to the stabilized $C_9H_{14}O_m$ products through multi-generation OH reactions, our conclusion that $C_{18}H_{28}O_x$ are multi-generation OH oxidation products still holds. Figure 4 shows the normalized signals of these abundant HOM dimers at different OH exposures.

(a)

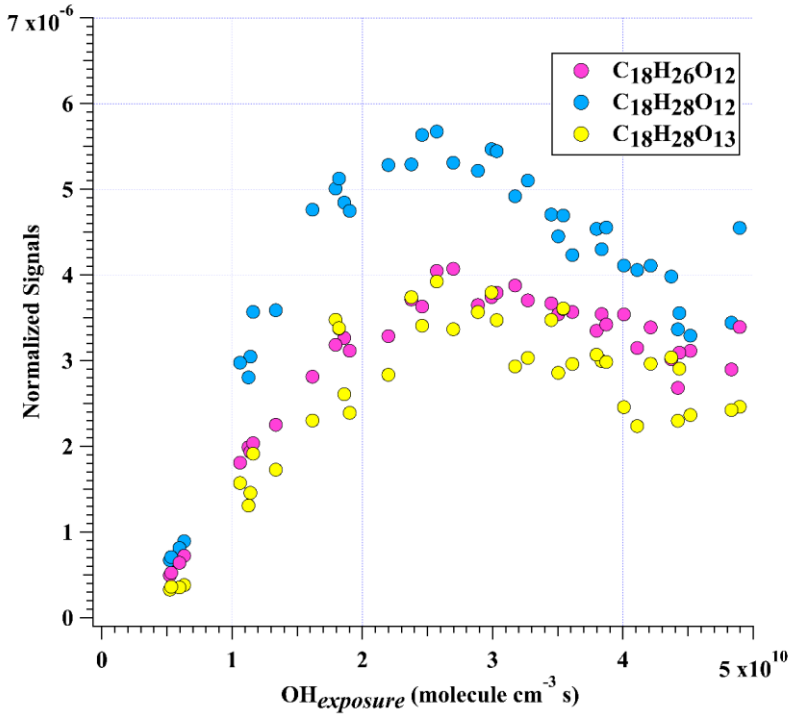

(b)

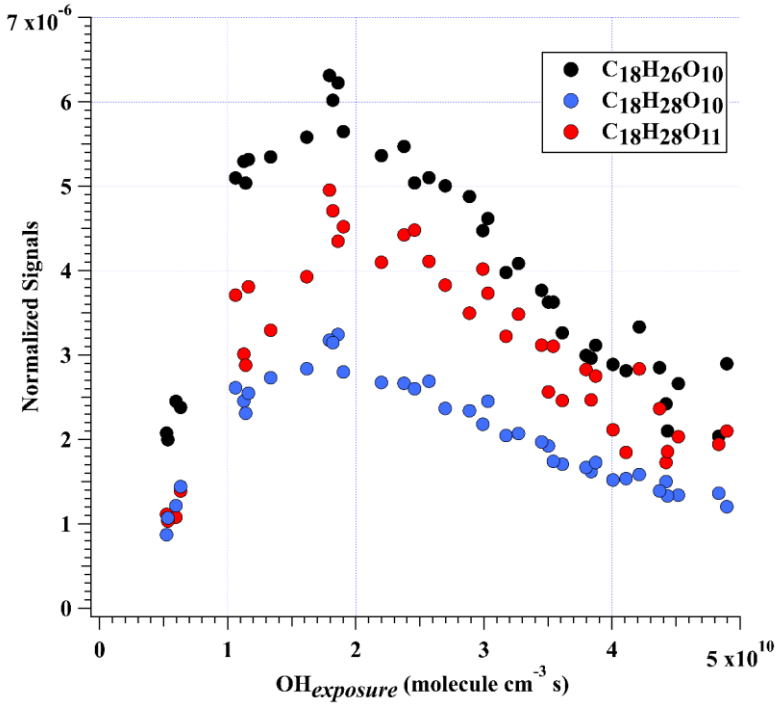

Figure 4. Normalized signals of (a) $C_{18}H_{26}O_{12}$, $C_{18}H_{28}O_{12}$, and $C_{18}H_{28}O_{13}$, and (b) $C_{18}H_{26}O_{10}$, $C_{18}H_{28}O_{10}$, and $C_{18}H_{28}O_{11}$ measured at the exit of OFR in our high [OH] experiments without NO_x as a function of OH exposure.

This decrease of dimer at relatively high OH exposures are likely due to the accelerated accretion reactions in the OFR, resulted by the high RO_2 concentrations. The HOM dimers are formed earlier compared to under ambient conditions and then can go through the further oxidation reactions. Note that this does not mean the maximum concentrations of HOM dimers will also accurately occur at the same OH exposures in the atmosphere, because the detailed appearance time of the maximum concentrations of HOM dimers is dependent on their formation rate and loss rate. In our experiments, the formation rate and loss rate were not accelerated equally. On the other hand, the loss pathways of HOM dimers were not exactly the same as the ambient. This series of experiments are not meant to specifically find out the detailed OH exposures when the maximum concentrations of HOM dimers will occur, but try to indicate how HOM dimers evolve with the increase of OH exposures. This work can be regarded as an indicator for the potential chemical fates of HOM dimers in the atmosphere if their survival time permitted. It should be noted that the gas-phase chemistry in the PAM OFR cannot be exactly the same as that in the ambient. Reactions of OH with OVOCs often lead to HO_2 formation, resulting in a HO_2:RO_2 ratio larger than 1 in the real atmosphere (Bianchi et al., 2019). A recent campaign conducted at a rural site in the Yangtze River Delta estimated that the local ratio of HO_2:RO_2, the latter of which was presumably derived from longer chain alkanes (> C_3), alkenes, and aromatic compounds, was around 1.66 (Ma et al., 2022). Such a

high HO_2:RO_2 ratio condition is typically difficult to be simulated in the laboratory experiments, as the precursors are usually hydrocarbons without any OVOCs (Peng and Jimenez, 2020). This is exactly the case for our experiments, but its influences on our conclusion were tiny, as have been discussed in the Section 3.1. Therefore, the difference in the distribution of products will not change our conclusion.

Such an active secondary OH chemistry is consistent with the fast OH reaction rates of HOMs. We take $C_{18}H_{26}O_8$ whose plausible structure is shown in Figure S4 as an example, which is the accretion product of two $C_9H_{13}O_5$·. Its OH reaction rate constant is estimated to be around 2.07×10^{-10} cm^3 $molecule^{-1}$ s^{-1} according to the structure-activity relationship (Jenkin et al., 2018b, a), whose details are provided in Supplementary Text S1. This rate is several times larger than that of 1,3,5-TMB, which enables a very active secondary OH chemistry in the system. MCM recommended an OH reaction rate of 1.28×10^{-10} cm^3 $molecule^{-1}$ s^{-1} for TM135BPOOH ($C_9H_{14}O_5$) and 1.00×10^{-10} cm^3 $molecule^{-1}$ s^{-1} for TM135OBPOH ($C_9H_{12}O_4$) (Jenkin et al., 2003). The OH reaction rate for $C_{18}H_{26}O_8$ should also be fast due to the C=C bonds in its structure, which is activated by the adjacent functionalities. Our calculation result is consistent with this estimation.

The distributions of C18 organonitrates also verified the extensive secondary reactions. The most abundant C18 organonitrate, $C_{18}H_{27}NO_{12}$ was a NO termination product of radical $C_{18}H_{27}O_{11}$·, which, as mentioned above, was the radical generated from the OH reaction with $C_{18}H_{26}O_8$. $C_{18}H_{27}NO_{12}$ can also be formed either by accretion between a $C_9H_{15}O_m$· radical and a $C_9H_{12}NO_m$· radical or accretion between a $C_9H_{13}O_m$· radical and a $C_9H_{14}NO_m$· radical. Both $C_9H_{15}O_m$· and $C_9H_{14}NO_m$· radicals are a typical multi-generation RO_2 and thus prove $C_{18}H_{27}NO_{12}$ is a multi-generation OH oxidation product. Other C18 organonitrates are believed to be formed in a similar pathway. Hence, plenty of organonitrates have been formed via the multi-generation OH reactions of first-generation stabilized products.

3.3 Oxidation products in low [OH] experiments

Given the larger sampling port, lower initial ozone concentrations, lower UV light intensities, and a better performance of mass spectrometer in this series of low [OH] experiments, a number of new species were detected in the 2nd-round experiments, including three typical termination reaction products of BPR, i.e., $C_9H_{14}O_4$, $C_9H_{14}O_5$, and $C_9H_{13}NO_6$, and a number of low volatile compounds, e.g., $C_9H_xO_{11}$ (x = 12 – 15). The distributions of oxidation products detected by nitrate CI-TOF in Exp. 2-3, 2-4, and 2-7, representative low [OH] experiments, are displayed in Figure 5. The detailed molecular formula and their contributions to total HOMs signals are provided in Tables S6 and S7.

In addition, certain C9 and C18 HOMs with lower DBE than typical first-generation products predicted by MCM (Saunders et al., 2003) or reported by previous studies (Berndt et al., 2018b), were detected in Exp. 2-3, 2-4, and 2-7, although [OH] in these experiments are much lower than those in the 1st-round experiments.

Observation of compounds with lower DBE in Exp. 2-3, 2-4, and 2-7 including HOM monomers with DBE lower than 3 and HOM dimers with DBE lower than 6, as well as monomer radicals with DBE lower than 3 including $C_9H_{15}O_m\cdot$ (m = 7 – 11) and $C_9H_{14}NO_9\cdot$, proves the re-initiation of OH oxidation of the stabilized products in experiments with atmospheric relevant [OH]. All the stabilized products and radicals depicted in the proposed mechanisms (Scheme 2 and Scheme 3) were detected in both Exp. 2-3 and Exp. 2-4, except for $C_9H_{15}O_9\cdot$ that was only detected in Exp. 2-3. This means that the proposed reaction pathways have already happened under atmospheric [OH] conditions with limited OH exposures. However, as we do not know the exact structures of these OOMs and radicals, the proposed reaction pathways are merely based on the chemical formulae detected by nitrate CIMS and nitrate CI-TOF and proposed according to the general mechanisms of OH addition reactions to the C=C bond. Other reaction pathways to generate these compounds or other isomers generated in these pathways are undoubtedly feasible.

A lot of compounds detected in the experiments without NO_x were not observed in the counterpart experiments with NO_x. We also did not detect decent signals of HOM dimers in the NO_x-present experiments in the 2nd-round experiments. Such a dramatic decrease in the abundance of HOM dimers after the introduction of NO_x into the aromatic oxidation system has been reported in several previous studies (Garmash et al., 2020; Wang et al., 2020b; Tsiligiannis et al., 2019). This might come from the dominant significance of NO + RO_2 reactions ($R8 - R9$) after the introduction of NO_x into system, making signals of certain HOMs from other channels lower than the detection limit of the instrument. The proportions of other reaction channels decreased, and were reassigned to the NO channel, as evidenced by the fact that most of observed oxidation products were organonitrates, which is in an excellent agreement with the modeled channel proportions in Section 3.1.

Many organonitrates were observed in both series of experiments. In the low [OH] experiments, the most significant compound was $C_9H_{13}NO_8$, whose formula matches the NO termination product of $C_9H_{13}O_7\cdot$, i.e., autoxidation product of BPR. The second most important compound, $C_9H_{14}N_2O_{10}$ in our low [OH] experiments, was the most significant product in the high [OH] experiments in presence of NO_x, whose formula matches the NO termination product of $C_9H_{14}NO_9\cdot$, i.e., the RO_2 formed via an OH addition to $C_9H_{13}NO_6$, the NO termination product of BPR. All of the products and radicals mentioned above were observed in Exp. 2-7,

as shown in Figure 5c. From the perspective of molecular formula, $C_9H_{14}N_2O_{10}$ is also one of the most frequently observed multi-nitrogen-containing compound in polluted atmospheres, whose seasonal variations show a good correlation with [OH] (Guo et al., 2022; Yang et al., 2023).

A comparison of relative abundances of C9 and C18 products under different [OH] levels is helpful for the elucidation of their formation pathways. The difference in product distributions between Exp. 2-3 ([OH] = ~1.69×10^7 molecule cm^{-3}) and Exp. 2-1 ([OH] = ~1.03×10^8 molecule cm^{-3}), as well as between Exp. 2-3 and Exp. 1-12 ([OH] = ~8.47×10^8 molecule cm^{-3}) is shown in Figure 6. The normalized abundance was obtained by normalizing all the products to the most abundant one in each experiment, i.e., $C_{18}H_{26}O_{10}$ in Exp. 2-1 and Exp. 2-3, and $C_9H_{14}O_7$ in Exp. 1-12. The changes in the normalized abundance were obtained by subtracting the normalized abundance in Exp. 2-1 from that in Exp. 2-3, and Exp. 1-12 from Exp. 2-3. As the [OH] and OH exposure increased, there was a noticeable rise in the relative abundance of more oxygenated compounds, which can be attributed to the larger proportion of multi-generation OH oxidation in high OH exposure experiments. This comparison demonstrates the capacity and potential of multi-generation OH oxidation to reduce DBE and elevate the oxygenated levels of oxidation products.

In conclusion, observation of the same low DBE compounds, i.e., DBE = 2, in both low [OH] and high [OH] experiments confirms the feasibility of the generation of HOMs under atmospheric relevant conditions. The detection of $C_9H_{14}O_5$, $C_9H_{15}O_8^{\cdot}$, $C_9H_{14}O_7$, $C_9H_{14}O_8$, $C_9H_{15}O_7^{\cdot}$, and $C_9H_{16}O_8$, and $C_9H_{14}O_6$, $C_9H_{15}O_9^{\cdot}$, $C_9H_{14}O_8$, $C_9H_{14}O_9$, $C_9H_{15}O_8^{\cdot}$, and $C_9H_{16}O_9$, in low [OH] experiments also confirms the potential existence of the proposed mechanisms, i.e., Scheme 2 and Scheme 3, respectively. Certainly, other potential formation pathways for these products are possible.

870 **(a)**

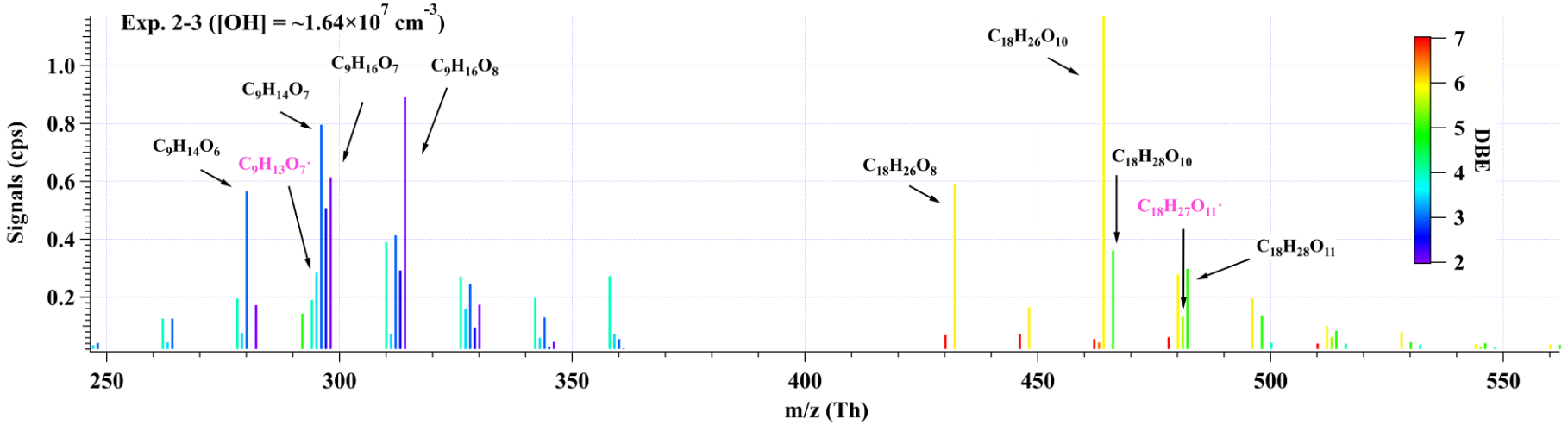

871

872 **(b)**

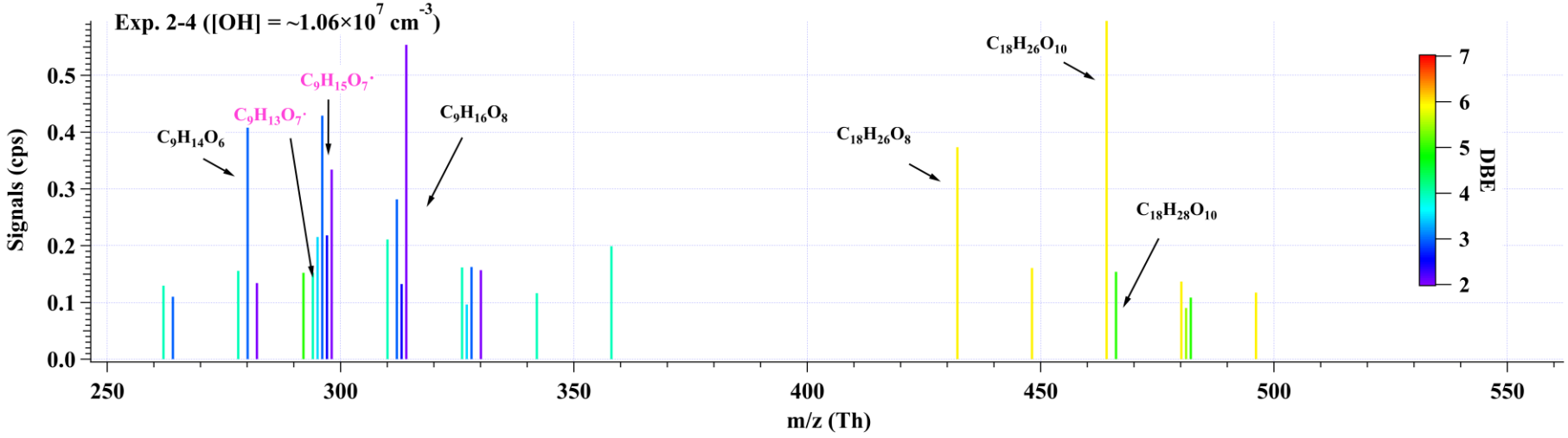
Exp. 2-4 ([OH] = ~1.06×10^7 cm^-3)
Signals (cps)
m/z (Th)
DBE
C9H14O6
C9H13O7·
C9H15O7·
C9H16O8
C18H26O8
C18H26O10
C18H28O10

873

(c)

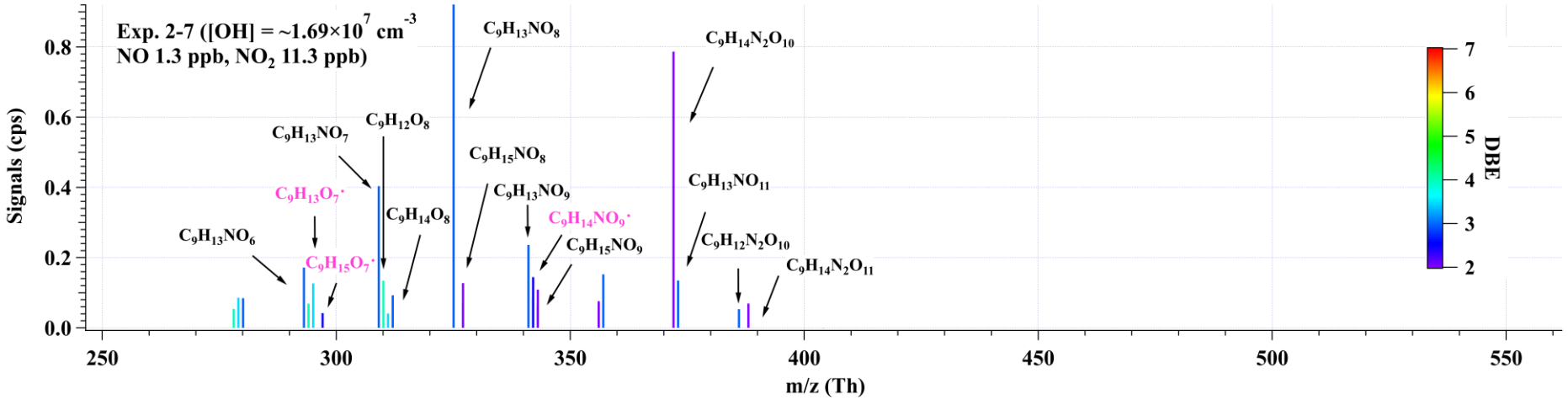

Figure 5. Distributions of C9 and C18 products detected by nitrate CI-TOF in (a) Exp. 2-3, (b) Exp. 2-4, and (c) Exp. 2-7. The reagent ion, NO_3^-, is omitted in the label for the molecular formula. Important radicals were labelled in pink. Note that no convinced signals of HOM dimers were observed in the 2nd-round experiments with NO_x.

881

882 **(a)**

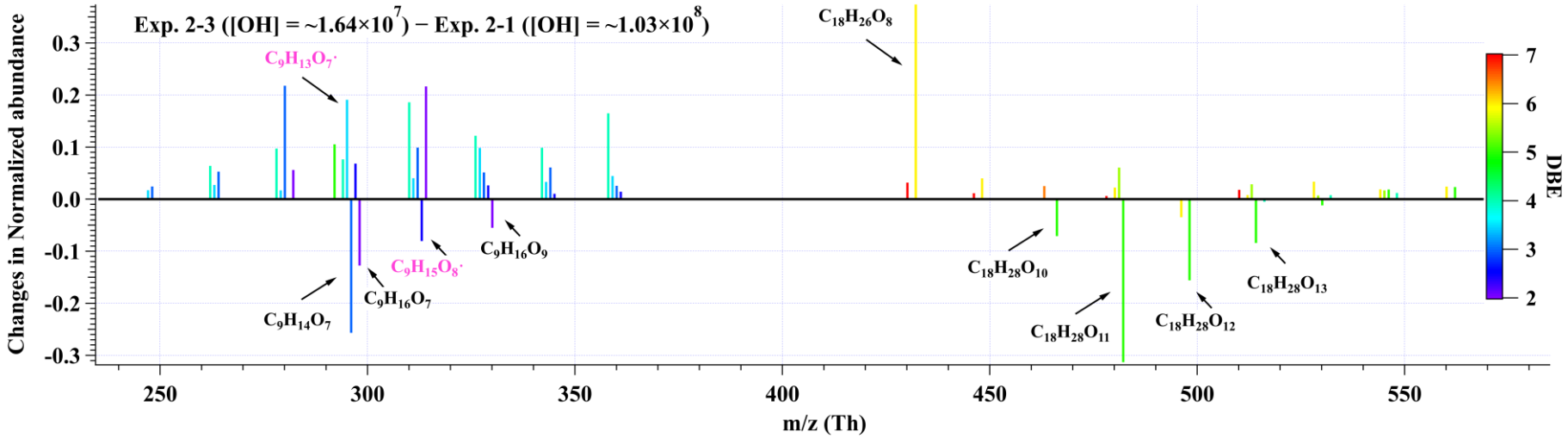

883

884 **(b)**

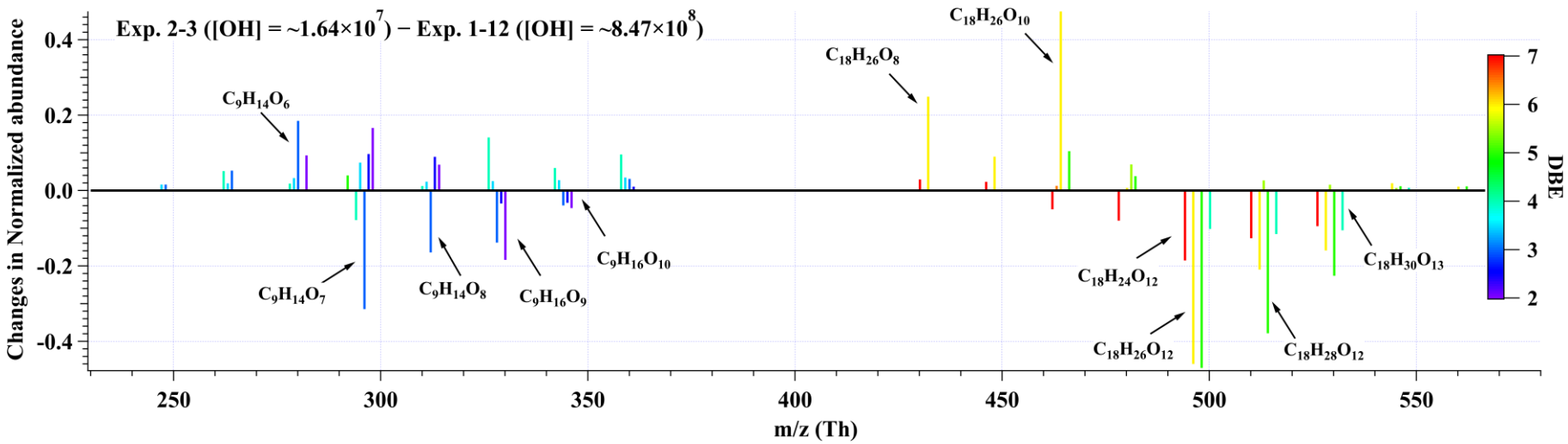

Figure 6. The changes in normalized abundance of C9 and C18 products observed by nitrate CI-TOF in (a) Exp.2-3 relative to Exp.2-1, and (b) Exp.2-3 relative to Exp.1-12. The reagent ion, NO_3^-, is omitted in the label. The normalized abundance was obtained by normalizing all the products to the most abundant one in each experiment, i.e., $C_{18}H_{26}O_{10}$ in Exp.2-1 and Exp.2-3, and $C_9H_{14}O_7$ in Exp.1-12.

4 Atmospheric Implications

This study highlights the influences of OH exposure on the distribution and evolution of 1,3,5-TMB-derived HOMs. Secondary OH reactions can influence HOMs' composition by directly reacting with the stabilized first-generation oxidation products, leading to enhanced formation of HOMs, if the stabilized, first-generation oxidation products could survive from condensation loss onto pre-existing particles. Observation of organonitrates generated in the NO experiments further confirmed the secondary OH oxidation. Due to the elevated abundance and the reduced volatility of HOMs, growth rates of newly formed nanoparticles in the presence of HOMs could be raised, especially in high-OH environments, which prevails in the summer noon. Substantially high concentrations of OH have been frequently observed in polluted environments during summer, e.g., megacities in China (Tan et al., 2019), and thus more active secondary OH reactions are expected compared to wintertime. As a plausible consequence, seasonal differences of HOMs and new particle formation (NPF) are resulted (Qiao et al., 2021; Yao et al., 2018; Guo et al., 2022). Furthermore, previous studies suggest that high concentrations of NO can suppress the formation of HOMs via the suppression of autoxidation (Pye et al., 2019), but the influences of such a suppression could have been overestimated, since secondary OH reactions can continue to oxidize the stabilized organonitrates. Our conclusions help to explain the existing gap between model prediction and ambient measurement on the HOMs concentrations (Qi et al., 2018), and to build a global HOMs simulation model.

Data availability. Data used in this work are available upon request from the corresponding authors.

Supplement. The supplement related to this article is available online.

Author contributions. LW and Yuwei Wang designed the experiments. Yuwei Wang and Chuang Li conducted the laboratory experiments. Yuwei Wang analyzed the data. Yuwei Wang and LW wrote the paper. All co-authors discussed the results and commented on the manuscript.

Competing interests. The authors declare that they have no conflict of interest.

Acknowledgments. This work was financially supported by the National Natural Science Foundation of China (21925601, 22127811). The authors declare no competing interests.

Yuwei Wang would like to thank Andrew T. Lambe, Peng Zhe, and Jose Jimenez for helpful discussions on PAM experiments.

References

Assaf, E., Song, B., Tomas, A., Schoemaecker, C., and Fittschen, C.: Rate Constant of the Reaction between CH 3 O 2 Radicals and OH Radicals Revisited , J. Phys. Chem. A, 120, 8923–8932, https://doi.org/10.1021/acs.jpca.6b07704, 2016.

Assaf, E., Tanaka, S., Kajii, Y., Schoemaecker, C., and Fittschen, C.: Rate constants of the reaction of C2–C4 peroxy radicals with OH radicals, Chem. Phys. Lett., 684, 245–249, https://doi.org/10.1016/j.cplett.2017.06.062, 2017.

Berndt, T., Mentler, B., Scholz, W., Fischer, L., Herrmann, H., Kulmala, M., and Hansel, A.: Accretion Product Formation from Ozonolysis and OH Radical Reaction of α-Pinene: Mechanistic Insight and the Influence of Isoprene and Ethylene, Environ. Sci. Technol., 52, 11069–11077, https://doi.org/10.1021/acs.est.8b02210, 2018a.

Berndt, T., Scholz, W., Mentler, B., Fischer, L., Herrmann, H., Kulmala, M., and Hansel, A.: Accretion Product Formation from Self- and Cross-Reactions of RO2 Radicals in the Atmosphere, Angew. Chemie - Int. Ed., 57, 3820–3824, https://doi.org/10.1002/anie.201710989, 2018b.

Bianchi, F., Kurtén, T., Riva, M., Mohr, C., Rissanen, M. P., Roldin, P., Berndt, T., Crounse, J. D., Wennberg, P. O., Mentel, T. F., Wildt, J., Junninen, H., Jokinen, T., Kulmala, M., Worsnop, D. R., Thornton, J. A., Donahue, N., Kjaergaard, H. G., and Ehn, M.: Highly Oxygenated Organic Molecules (HOM) from Gas-Phase Autoxidation Involving Peroxy Radicals: A Key Contributor to Atmospheric Aerosol, Chem. Rev., 119, 3472–3509, https://doi.org/10.1021/acs.chemrev.8b00395, 2019.

Bossolasco, A., Faragó, E. P., Schoemaecker, C., and Fittschen, C.: Rate constant of the reaction between CH3O2 and OH radicals, Chem. Phys. Lett., 593, 7–13, https://doi.org/10.1016/j.cplett.2013.12.052, 2014.

Brune, W. H.: The Chamber Wall Index for Gas-Wall Interactions in Atmospheric Environmental Enclosures, Environ. Sci. Technol., 53, 3645–3652, https://doi.org/10.1021/acs.est.8b06260, 2019.

Caravan, R. L., Khan, M. A. H., Zádor, J., Sheps, L., Antonov, I. O., Rotavera, B., Ramasesha, K., Au, K., Chen, M. W., Rösch, D., Osborn, D. L., Fittschen, C., Schoemaecker, C., Duncianu, M., Grira, A., Dusanter, S., Tomas, A., Percival, C. J., Shallcross, D. E., and Taatjes, C. A.: The reaction of hydroxyl and methylperoxy radicals is not a major source of atmospheric methanol, Nat. Commun., 9, 1–9, https://doi.org/10.1038/s41467-018-06716-x, 2018.

Cheng, X., Chen, Q., Li, Y. J., Zheng, Y., Liao, K., and Huang, G.: Highly Oxygenated Organic Molecules Produced by the Oxidation of Benzene and Toluene in a Wide Range of OH Exposure and NOx Conditions, Atmos. Chem. Phys., 1–23, https://doi.org/10.5194/acp-2021-201, 2021.

Crounse, J. D., Nielsen, L. B., Jørgensen, S., Kjaergaard, H. G., and Wennberg, P. O.: Autoxidation of organic compounds in the atmosphere, J. Phys. Chem. Lett., 4, 3513–3520, https://doi.org/10.1021/jz4019207, 2013.

Deng, C., Fu, Y., Dada, L., Yan, C., Cai, R., Yang, D., Zhou, Y., Yin, R., Lu, Y., Li, X., Qiao, X., Fan, X., Nie, W., Kontkanen, J., Kangasluoma, J., Chu, B., Ding, A., Kerminen, V. M., Paasonen, P., Worsnop, D. R., Bianchi, F., Liu, Y., Zheng, J., Wang, L., Kulmala, M., and

Jiang, J.: Seasonal characteristics of new particle formation and growth in urban Beijing, Environ. Sci. Technol., 54, 8547–8557, https://doi.org/10.1021/acs.est.0c00808, 2020.
Ehn, M., Thornton, J. A., Kleist, E., Sipilä, M., Junninen, H., Pullinen, I., Springer, M., Rubach, F., Tillmann, R., Lee, B., Lopez-Hilfiker, F., Andres, S., Acir, I. H., Rissanen, M., Jokinen, T., Schobesberger, S., Kangasluoma, J., Kontkanen, J., Nieminen, T., Kurtén, T., Nielsen, L. B., Jørgensen, S., Kjaergaard, H. G., Canagaratna, M., Maso, M. D., Berndt, T., Petäjä, T., Wahner, A., Kerminen, V. M., Kulmala, M., Worsnop, D. R., Wildt, J., and Mentel, T. F.: A large source of low-volatility secondary organic aerosol, Nature, 506, 476–479, https://doi.org/10.1038/nature13032, 2014.
Eisele, F. L. and Tanner, D. J.: Measurement of the gas phase concentration of H 2 SO 4 and methane sulfonic acid and estimates of H 2 SO 4 production and loss in the atmosphere, J. Geophys. Res. Atmos., 98, 9001–9010, https://doi.org/10.1029/93JD00031, 1993.
Fittschen, C.: The reaction of peroxy radicals with OH radicals, Chem. Phys. Lett., 725, 102–108, https://doi.org/10.1016/j.cplett.2019.04.002, 2019.
Fuller, E. N., Schettler, P. D., and Giddings, J. C.: A new method for prediction of binary gas-phase diffusion coefficients, Ind. Eng. Chem., 58, 18–27, https://doi.org/10.1021/ie50677a007, 1966.
Garmash, O., Rissanen, M. P., Pullinen, I., Schmitt, S., Kausiala, O., Tillmann, R., Zhao, D., Percival, C., Bannan, T. J., Priestley, M., Hallquist, Å. M., Kleist, E., Kiendler-Scharr, A., Hallquist, M., Berndt, T., McFiggans, G., Wildt, J., Mentel, T. F., and Ehn, M.: Multi-generation OH oxidation as a source for highly oxygenated organic molecules from aromatics, Atmos. Chem. Phys., 20, 515–537, https://doi.org/10.5194/acp-20-515-2020, 2020.
Guo, Y., Yan, C., Liu, Y., Qiao, X., Zheng, F., Zhang, Y., Zhou, Y., Li, C., Fan, X., Lin, Z., Feng, Z., Zhang, Y., Zheng, P., Tian, L., Nie, W., Wang, Z., Huang, D., Daellenbach, K. R., Yao, L., Dada, L., Bianchi, F., Jiang, J., Liu, Y., Kerminen, V. M., and Kulmala, M.: Seasonal variation in oxygenated organic molecules in urban Beijing and their contribution to secondary organic aerosol, Atmos. Chem. Phys., 22, 10077–10097, https://doi.org/10.5194/acp-22-10077-2022, 2022.
Heinritzi, M., Simon, M., Steiner, G., Wagner, A. C., Kürten, A., Hansel, A., and Curtius, J.: Characterization of the mass-dependent transmission efficiency of a CIMS, Atmos. Meas. Tech., 9, 1449–1460, https://doi.org/10.5194/amt-9-1449-2016, 2016.
Hyttinen, N., Kupiainen-Määttä, O., Rissanen, M. P., Muuronen, M., Ehn, M., and Kurtén, T.: Modeling the Charging of Highly Oxidized Cyclohexene Ozonolysis Products Using Nitrate-Based Chemical Ionization, J. Phys. Chem. A, 119, 6339–6345, https://doi.org/10.1021/acs.jpca.5b01818, 2015.
Iyer, S., Kumar, A., Savolainen, A., Barua, S., Daub, C., Pichelstorfer, L., Roldin, P., Garmash, O., Seal, P., Kurtén, T., and Rissanen, M.: Molecular rearrangement of bicyclic peroxy radicals is a key route to aerosol from aromatics, Nat. Commun., 14, 4984, https://doi.org/10.1038/s41467-023-40675-2, 2023.
Jacob, D. J.: Introduction to atmospheric chemistry, Princeton, 1999.
Jenkin, M. E., Saunders, S. M., Wagner, V., and Pilling, M. J.: Protocol for the development of the Master Chemical Mechanism, MCM v3 (Part B): tropospheric degradation of aromatic volatile organic compounds, Atmos. Chem. Phys., 3, 181–193, https://doi.org/10.5194/acp-3-181-2003, 2003.

Jenkin, M. E., Valorso, R., Aumont, B., Rickard, A. R., and Wallington, T. J.: Estimation of rate coefficients and branching ratios for gas-phase reactions of OH with aliphatic organic compounds for use in automated mechanism construction, 9297–9328 pp., https://doi.org/10.5194/acp-18-9297-2018, 2018a.

Jenkin, M. E., Valorso, R., Aumont, B., Rickard, A. R., and Wallington, T. J.: Estimation of rate coefficients and branching ratios for gas-phase reactions of OH with aromatic organic compounds for use in automated mechanism construction, Atmos. Chem. Phys., 18, 9329–9349, https://doi.org/10.5194/acp-18-9329-2018, 2018b.

Keller-Rudek, H., Moortgat, G. K., Sander, R., and Sörensen, R.: The MPI-Mainz UV/VIS spectral atlas of gaseous molecules of atmospheric interest, Earth Syst. Sci. Data, 5, 365–373, https://doi.org/10.5194/essd-5-365-2013, 2013.

Knap, H. C. and Jørgensen, S.: Rapid Hydrogen Shift Reactions in Acyl Peroxy Radicals, J. Phys. Chem. A, 121, 1470–1479, https://doi.org/10.1021/acs.jpca.6b12787, 2017.

Krechmer, J., Lopez-Hilfiker, F., Koss, A., Hutterli, M., Stoermer, C., Deming, B., Kimmel, J., Warneke, C., Holzinger, R., Jayne, J., Worsnop, D., Fuhrer, K., Gonin, M., and De Gouw, J.: Evaluation of a New Reagent-Ion Source and Focusing Ion− Molecule Reactor for Use in Proton-Transfer-Reaction Mass Spectrometry, Anal. Chem., 90, 12011–12018, https://doi.org/10.1021/acs.analchem.8b02641, 2018.

Lambe, A., Massoli, P., Zhang, X., Canagaratna, M., Nowak, J., Daube, C., Yan, C., Nie, W., Onasch, T., Jayne, J., Kolb, C., Davidovits, P., Worsnop, D., and Brune, W.: Controlled nitric oxide production via O(1D) + N2O reactions for use in oxidation flow reactor studies, Atmos. Meas. Tech., 10, 2283–2298, https://doi.org/10.5194/amt-10-2283-2017, 2017.

Lambe, A., Krechmer, J., Peng, Z., Casar, J., Carrasquillo, A., Raff, J., Jimenez, J., and Worsnop, D.: HO x and NO x production in oxidation flow reactors via photolysis of, 1–22, 2018.

Lambe, A. T., Ahern, A. T., Williams, L. R., Slowik, J. G., Wong, J. P. S., Abbatt, J. P. D., Brune, W. H., Ng, N. L., Wright, J. P., Croasdale, D. R., Worsnop, D. R., Davidovits, P., and Onasch, T. B.: Characterization of aerosol photooxidation flow reactors: heterogeneous oxidation, secondary organic aerosol formation and cloud condensation nuclei activity measurements, Atmos. Meas. Tech, 4, 445–461, https://doi.org/10.5194/amt-4-445-2011, 2011.

Lambe, A. T., Chhabra, P. S., Onasch, T. B., Brune, W. H., Hunter, J. F., Kroll, J. H., Cummings, M. J., Brogan, J. F., Parmar, Y., Worsnop, D. R., Kolb, C. E., and Davidovits, P.: Effect of oxidant concentration, exposure time, and seed particles on secondary organic aerosol chemical composition and yield, Atmos. Chem. Phys., 15, 3063–3075, https://doi.org/10.5194/acp-15-3063-2015, 2015.

Lehtipalo, K., Yan, C., Dada, L., Bianchi, F., Xiao, M., Wagner, R., Stolzenburg, D., Ahonen, L. R., Amorim, A., Baccarini, A., Bauer, P. S., Baumgartner, B., Bergen, A., Bernhammer, A. K., Breitenlechner, M., Brilke, S., Buchholz, A., Mazon, S. B., Chen, D., Chen, X., Dias, A., Dommen, J., Draper, D. C., Duplissy, J., Ehn, M., Finkenzeller, H., Fischer, L., Frege, C., Fuchs, C., Garmash, O., Gordon, H., Hakala, J., He, X., Heikkinen, L., Heinritzi, M., Helm, J. C., Hofbauer, V., Hoyle, C. R., Jokinen, T., Kangasluoma, J., Kerminen, V. M., Kim, C., Kirkby, J., Kontkanen, J., Kürten, A., Lawler, M. J., Mai, H., Mathot, S., Mauldin, R. L., Molteni, U., Nichman, L., Nie, W., Nieminen, T., Ojdanic, A., Onnela, A., Passananti, M.,

Petäjä, T., Piel, F., Pospisilova, V., Quéléver, L. L. J., Rissanen, M. P., Rose, C., Sarnela, N., Schallhart, S., Schuchmann, S., Sengupta, K., Simon, M., Sipilä, M., Tauber, C., Tomé, A., Tröstl, J., Väisänen, O., Vogel, A. L., Volkamer, R., Wagner, A. C., Wang, M., Weitz, L., Wimmer, D., Ye, P., Ylisirniö, A., Zha, Q., Carslaw, K. S., Curtius, J., Donahue, N. M., Flagan, R. C., Hansel, A., Riipinen, I., Virtanen, A., Winkler, P. M., Baltensperger, U., Kulmala, M., and Worsnop, D. R.: Multicomponent new particle formation from sulfuric acid, ammonia, and biogenic vapors, Sci. Adv., 4, 1–10, https://doi.org/10.1126/sciadv.aau5363, 2018.

Li, R., Palm, B. B., Ortega, A. M., Hlywiak, J., Hu, W., Peng, Z., Day, D. A., Knote, C., Brune, W. H., De Gouw, J. A., and Jimenez, J. L.: Modeling the radical chemistry in an oxidation flow reactor: Radical formation and recycling, sensitivities, and the OH exposure estimation equation, J. Phys. Chem. A, 119, 4418–4432, https://doi.org/10.1021/jp509534k, 2015.

Lu, K. D., Rohrer, F., Holland, F., Fuchs, H., Bohn, B., Brauers, T., Chang, C. C., Häseler, R., Hu, M., Kita, K., Kondo, Y., Li, X., Lou, S. R., Nehr, S., Shao, M., Zeng, L. M., Wahner, A., Zhang, Y. H., and Hofzumahaus, A.: Observation and modelling of OH and HO2 concentrations in the Pearl River Delta 2006: A missing OH source in a VOC rich atmosphere, Atmos. Chem. Phys., 12, 1541–1569, https://doi.org/10.5194/acp-12-1541-2012, 2012.

Ma, X., Tan, Z., Lu, K., Yang, X., Chen, X., Wang, H., Chen, S., Fang, X., Li, S., Li, X., Liu, J., Liu, Y., Lou, S., Qiu, W., Wang, H., Zeng, L., and Zhang, Y.: OH and HO2 radical chemistry at a suburban site during the EXPLORE-YRD campaign in 2018, Atmos. Chem. Phys., 22, 7005–7028, https://doi.org/10.5194/acp-22-7005-2022, 2022.

McMurry, P. H. and Grosjean, D.: Gas and Aerosol Wall Losses in Teflon Film Smog Chambers, Environ. Sci. Technol., 19, 1176–1182, https://doi.org/10.1021/es00142a006, 1985.

Mehra, A., Wang, Y., E. Krechmer, J., Lambe, A., Majluf, F., A. Morris, M., Priestley, M., J. Bannan, T., J. Bryant, D., L. Pereira, K., F. Hamilton, J., R. Rickard, A., J. Newland, M., Stark, H., Croteau, P., T. Jayne, J., R. Worsnop, D., R. Canagaratna, M., Wang, L., and Coe, H.: Evaluation of the chemical composition of gas- And particle-phase products of aromatic oxidation, Atmos. Chem. Phys., 20, 9783–9803, https://doi.org/10.5194/acp-20-9783-2020, 2020.

Mentel, T. F., Springer, M., Ehn, M., Kleist, E., Pullinen, I., Kurtén, T., Rissanen, M., Wahner, A., and Wildt, J.: Formation of highly oxidized multifunctional compounds: Autoxidation of peroxy radicals formed in the ozonolysis of alkenes - Deduced from structure-product relationships, Atmos. Chem. Phys., 15, 6745–6765, https://doi.org/10.5194/acp-15-6745-2015, 2015.

Mohr, C., Thornton, J. A., Heitto, A., Lopez-hil, F. D., Lutz, A., Riipinen, I., Hong, J., Donahue, N. M., Hallquist, M., Petäjä, T., Kulmala, M., and Yli-juuti, T.: Molecular identification of organic vapors driving atmospheric nanoparticle growth, Nat. Commun., 1–7, https://doi.org/10.1038/s41467-019-12473-2, 2019.

Molteni, U., Bianchi, F., Klein, F., Haddad, I. El, Frege, C., Rossi, M. J., Dommen, J., and Baltensperger, U.: Formation of highly oxygenated organic molecules from aromatic

compounds, Atmos. Chem. Phys, 18, 1909–1921, https://doi.org/10.5194/acp-18-1909-2018, 2018.
Müller, J. F., Liu, Z., Nguyen, V. S., Stavrakou, T., Harvey, J. N., and Peeters, J.: The reaction of methyl peroxy and hydroxyl radicals as a major source of atmospheric methanol, Nat. Commun., 7, 1–11, https://doi.org/10.1038/ncomms13213, 2016.
Ng, N. L., Canagaratna, M. R., Zhang, Q., Jimenez, J. L., Tian, J., Ulbrich, I. M., Kroll, J. H., Docherty, K. S., Chhabra, P. S., Bahreini, R., Murphy, S. M., Seinfeld, J. H., Hildebrandt, L., Donahue, N. M., Decarlo, P. F., Lanz, V. A., Prévôt, A. S. H., Dinar, E., Rudich, Y., and Worsnop, D. R.: Organic aerosol components observed in Northern Hemispheric datasets from Aerosol Mass Spectrometry, Atmos. Chem. Phys., 10, 4625–4641, https://doi.org/10.5194/acp-10-4625-2010, 2010.
Orlando, J. J. and Tyndall, G. S.: Laboratory studies of organic peroxy radical chemistry: An overview with emphasis on recent issues of atmospheric significance, Chem. Soc. Rev., 41, 6294–6317, https://doi.org/10.1039/c2cs35166h, 2012.
Otkjær, R. V., Jakobsen, H. H., Tram, C. M., and Kjaergaard, H. G.: Calculated Hydrogen Shift Rate Constants in Substituted Alkyl Peroxy Radicals, J. Phys. Chem. A, 122, 8665–8673, https://doi.org/10.1021/acs.jpca.8b06223, 2018.
Palm, B. B., Campuzano-Jost, P., Ortega, A. M., Day, D. A., Kaser, L., Jud, W., Karl, T., Hansel, A., Hunter, J. F., Cross, E. S., Kroll, J. H., Peng, Z., Brune, W. H., and Jimenez, J. L.: In situ secondary organic aerosol formation from ambient pine forest air using an oxidation flow reactor, Atmos. Chem. Phys., 16, 2943–2970, https://doi.org/10.5194/acp-16-2943-2016, 2016.
Peng, Z. and Jimenez, J. L.: Radical chemistry in oxidation flow reactors for atmospheric chemistry research, Chem. Soc. Rev., 49, 2570–2616, https://doi.org/10.1039/c9cs00766k, 2020.
Peng, Z., Day, D. A., Ortega, A. M., Palm, B. B., Hu, W., Stark, H., Li, R., Tsigaridis, K., Brune, W. H., and Jimenez, J. L.: Non-OH chemistry in oxidation flow reactors for the study of atmospheric chemistry systematically examined by modeling, Atmos. Chem. Phys., 16, 4283–4305, https://doi.org/10.5194/acp-16-4283-2016, 2016.
Praske, E., Otkjær, R. V., Crounse, J. D., Hethcox, J. C., Stoltz, B. M., Kjaergaard, H. G., and Wennberg, P. O.: Atmospheric autoxidation is increasingly important in urban and suburban North America, Proc. Natl. Acad. Sci. U. S. A., 115, 64–69, https://doi.org/10.1073/pnas.1715540115, 2018.
Pye, H. O. T., D'Ambro, E. L., Lee, B. H., Schobesberger, S., Takeuchi, M., Zhao, Y., Lopez-Hilfiker, F., Liu, J., Shilling, J. E., Xing, J., Mathur, R., Middlebrook, A. M., Liao, J., Welti, A., Graus, M., Warneke, C., de Gouw, J. A., Holloway, J. S., Ryerson, T. B., Pollack, I. B., and Thornton, J. A.: Anthropogenic enhancements to production of highly oxygenated molecules from autoxidation, Proc. Natl. Acad. Sci. U. S. A., 116, 6641–6646, https://doi.org/10.1073/pnas.1810774116, 2019.
Qi, X., Ding, A., Roldin, P., Xu, Z., Zhou, P., Sarnela, N., Nie, W., Huang, X., Rusanen, A., Ehn, M., Rissanen, M. P., Petäjä, T., Kulmala, M., and Boy, M.: Modelling studies of HOMs and their contributions to new particle formation and growth: comparison of boreal forest in Finland and a polluted environment in China, Atmos. Chem. Phys, 18, 11779–11791, https://doi.org/10.5194/acp-18-11779-2018, 2018.

Qiao, X., Yan, C., Li, X., Guo, Y., Yin, R., Deng, C., Li, C., Nie, W., Wang, M., Cai, R., Huang, D., Wang, Z., Yao, L., Worsnop, D. R., Bianchi, F., Liu, Y., Donahue, N. M., Kulmala, M., and Jiang, J.: Contribution of Atmospheric Oxygenated Organic Compounds to Particle Growth in an Urban Environment, Environ. Sci. Technol., https://doi.org/10.1021/acs.est.1c02095, 2021.

Qu, H., Wang, Y., Zhang, R., Liu, X., Huey, L. G., Sjostedt, S., Zeng, L., Lu, K., Wu, Y., Shao, M., Hu, M., Tan, Z., Fuchs, H., Broch, S., Wahner, A., Zhu, T., and Zhang, Y.: Chemical Production of Oxygenated Volatile Organic Compounds Strongly Enhances Boundary-Layer Oxidation Chemistry and Ozone Production, Environ. Sci. Technol., 55, 13718–13727, https://doi.org/10.1021/acs.est.1c04489, 2021.

Saunders, S. M., Jenkin, M. E., Derwent, R. G., and Pilling, M. J.: Protocol for the development of the Master Chemical Mechanism, MCM v3 (Part A): Tropospheric degradation of non-aromatic volatile organic compounds, Atmos. Chem. Phys., 3, 161–180, https://doi.org/10.5194/acp-3-161-2003, 2003.

Stolzenburg, D., Fischer, L., Vogel, A. L., Heinritzi, M., Schervish, M., Simon, M., Wagner, A. C., Dada, L., Ahonen, L. R., Amorim, A., Baccarini, A., Bauer, P. S., Baumgartner, B., Bergen, A., Bianchi, F., Breitenlechner, M., Brilke, S., Mazon, S. B., Chen, D., Dias, A., Draper, D. C., Duplissy, J., Haddad, I. El, Finkenzeller, H., Frege, C., Fuchs, C., Garmash, O., Gordon, H., He, X., Helm, J., Hofbauer, V., Hoyle, C. R., Kim, C., Kirkby, J., Kontkanen, J., Kürten, A., Lampilahti, J., Lawler, M., Lehtipalo, K., Leiminger, M., Mai, H., Mathot, S., Mentler, B., Molteni, U., Nie, W., Nieminen, T., Nowak, J. B., Ojdanic, A., Onnela, A., Passananti, M., Petäjä, T., Quéléver, L. L. J., Rissanen, M. P., Sarnela, N., Schallhart, S., Tauber, C., Tomé, A., Wagner, R., Wang, M., Weitz, L., Wimmer, D., Xiao, M., Yan, C., Ye, P., Zha, Q., Baltensperger, U., Curtius, J., Dommen, J., Flagan, R. C., Kulmala, M., Smith, J. N., Worsnop, D. R., Hansel, A., Donahue, N. M., and Winkler, P. M.: Rapid growth of organic aerosol nanoparticles over a wide tropospheric temperature range, Proc. Natl. Acad. Sci. U. S. A., 115, 9122–9127, https://doi.org/10.1073/pnas.1807604115, 2018.

Tan, Z., Fuchs, H., Lu, K., Hofzumahaus, A., Bohn, B., Broch, S., Dong, H., Gomm, S., Häseler, R., He, L., Holland, F., Li, X., Liu, Y., Lu, S., Rohrer, F., Shao, M., Wang, B., Wang, M., Wu, Y., Zeng, L., Zhang, Y., Wahner, A., and Zhang, Y.: Radical chemistry at a rural site (Wangdu) in the North China Plain: Observation and model calculations of OH, HO2 and RO2 radicals, Atmos. Chem. Phys., 17, 663–690, https://doi.org/10.5194/acp-17-663-2017, 2017.

Tan, Z., Rohrer, F., Lu, K., Ma, X., Bohn, B., Broch, S., Dong, H., Fuchs, H., Gkatzelis, G. I., Hofzumahaus, A., Holland, F., Li, X., Liu, Y., Liu, Y., Novelli, A., Shao, M., Wang, H., Wu, Y., Zeng, L., Hu, M., Kiendler-Scharr, A., Wahner, A., and Zhang, Y.: Wintertime photochemistry in Beijing: Observations of ROx radical concentrations in the North China Plain during the BEST-ONE campaign, Atmos. Chem. Phys., https://doi.org/10.5194/acp-18-12391-2018, 2018.

Tan, Z., Lu, K., Jiang, M., Su, R., Wang, H., Lou, S., Fu, Q., Zhai, C., Tan, Q., Yue, D., Chen, D., Wang, Z., Xie, S., Zeng, L., and Zhang, Y.: Daytime atmospheric oxidation capacity in four Chinese megacities during the photochemically polluted season: A case study based on box model simulation, Atmos. Chem. Phys., 19, 3493–3513, https://doi.org/10.5194/acp-19-3493-2019, 2019.

Tröstl, J., Chuang, W. K., Gordon, H., Heinritzi, M., Yan, C., Molteni, U., Ahlm, L., Frege, C., Bianchi, F., Wagner, R., Simon, M., Lehtipalo, K., Williamson, C., Craven, J. S., Duplissy, J., Adamov, A., Almeida, J., Bernhammer, A. K., Breitenlechner, M., Brilke, S., Dias, A., Ehrhart, S., Flagan, R. C., Franchin, A., Fuchs, C., Guida, R., Gysel, M., Hansel, A., Hoyle, C. R., Jokinen, T., Junninen, H., Kangasluoma, J., Keskinen, H., Kim, J., Krapf, M., Kürten, A., Laaksonen, A., Lawler, M., Leiminger, M., Mathot, S., Möhler, O., Nieminen, T., Onnela, A., Petäjä, T., Piel, F. M., Miettinen, P., Rissanen, M. P., Rondo, L., Sarnela, N., Schobesberger, S., Sengupta, K., Sipilä, M., Smith, J. N., Steiner, G., Tomè, A., Virtanen, A., Wagner, A. C., Weingartner, E., Wimmer, D., Winkler, P. M., Ye, P., Carslaw, K. S., Curtius, J., Dommen, J., Kirkby, J., Kulmala, M., Riipinen, I., Worsnop, D. R., Donahue, N. M., and Baltensperger, U.: The role of low-volatility organic compounds in initial particle growth in the atmosphere, Nature, 533, 527–531, https://doi.org/10.1038/nature18271, 2016.

Tsiligiannis, E., Hammes, J., Salvador, C. M., Mentel, T. F., and Hallquist, M.: Effect of NOx on 1,3,5-trimethylbenzene (TMB) oxidation product distribution and particle formation, Atmos. Chem. Phys., 19, 15073–15086, https://doi.org/10.5194/acp-19-15073-2019, 2019.

Vereecken, L.: Reaction Mechanisms for the Atmospheric Oxidation of Monocyclic Aromatic Compounds, Adv. Atmos. Chem., 377–527, https://doi.org/10.1142/9789813271838_0006, 2019.

Wang, L., Wu, R., and Xu, C.: Atmospheric oxidation mechanism of benzene. Fates of alkoxy radical intermediates and revised mechanism, J. Phys. Chem. A, 117, 14163–14168, https://doi.org/10.1021/jp4101762, 2013.

Wang, M., Chen, D., Xiao, M., Ye, Q., Stolzenburg, D., Hofbauer, V., Ye, P., Vogel, A. L., Mauldin, R. L., Amorim, A., Baccarini, A., Baumgartner, B., Brilke, S., Dada, L., Dias, A., Duplissy, J., Finkenzeller, H., Garmash, O., He, X. C., Hoyle, C. R., Kim, C., Kvashnin, A., Lehtipalo, K., Fischer, L., Molteni, U., Petäjä, T., Pospisilova, V., Quéléver, L. L. J., Rissanen, M., Simon, M., Tauber, C., Tomé, A., Wagner, A. C., Weitz, L., Volkamer, R., Winkler, P. M., Kirkby, J., Worsnop, D. R., Kulmala, M., Baltensperger, U., Dommen, J., El-Haddad, I., and Donahue, N. M.: Photo-oxidation of Aromatic Hydrocarbons Produces Low-Volatility Organic Compounds, Environ. Sci. Technol., 54, 7911–7921, https://doi.org/10.1021/acs.est.0c02100, 2020a.

Wang, S., Wu, R., Berndt, T., Ehn, M., and Wang, L.: Formation of Highly Oxidized Radicals and Multifunctional Products from the Atmospheric Oxidation of Alkylbenzenes, Environ. Sci. Technol., 51, 8442–8449, https://doi.org/10.1021/acs.est.7b02374, 2017.

Wang, W., Yuan, B., Peng, Y., Su, H., Cheng, Y., and Yang, S.: Direct observations indicate photodegradable oxygenated VOCs as larger contributors to radicals and ozone production in the atmosphere, Atmos. Chem. Phys., 1–28, 2022.

Wang, Y., Mehra, A., Krechmer, J. E., Yang, G., Hu, X., Lu, Y., Lambe, A., Canagaratna, M., Chen, J., Worsnop, D., Coe, H., and Wang, L.: Oxygenated products formed from OH-initiated reactions of trimethylbenzene: autoxidation and accretion, Atmos. Chem. Phys., 20, 9563–9579, https://doi.org/10.5194/acp-20-9563-2020, 2020b.

Whalley, L. K., Slater, E. J., Woodward-Massey, R., Ye, C., Lee, J. D., Squires, F., Hopkins, J. R., Dunmore, R. E., Shaw, M., Hamilton, J. F., Lewis, A. C., Mehra, A., Worrall, S. D., Bacak, A., Bannan, T. J., Coe, H., Percival, C. J., Ouyang, B., Jones, R. L., Crilley, L. R., Kramer, L. J., Bloss, W. J., Vu, T., Kotthaus, S., Grimmond, S., Sun, Y., Xu, W., Yue, S.,

Ren, L., Joe, W., Nicholas Hewitt, C., Wang, X., Fu, P., and Heard, D. E.: Evaluating the sensitivity of radical chemistry and ozone formation to ambient VOCs and NOxin Beijing, Atmos. Chem. Phys., 21, 2125–2147, https://doi.org/10.5194/acp-21-2125-2021, 2021.
Xu, L., Møller, K. H., Crounse, J. D., Kjaergaard, H. G., and Wennberg, P. O.: New insights into the radical chemistry and product distribution in the OH-initiated oxidation of benzene, Environ. Sci. Technol., 54, 13467–13477, https://doi.org/10.1021/acs.est.0c04780, 2020.
Yan, C., Kocevska, S., and Krasnoperov, L. N.: Kinetics of the Reaction of CH3O2 Radicals with OH Studied over the 292-526 K Temperature Range, J. Phys. Chem. A, 120, 6111–6121, https://doi.org/10.1021/acs.jpca.6b04213, 2016.
Yang, C., Yao, N., Xu, L., Chen, G., Wang, Y., Fan, X., Zhou, P., Clusius, P., Tham, Y. J., Lin, Z., Chen, Y., Li, M., Hong, Y., and Chen, J.: Molecular Composition of Anthropogenic Oxygenated Organic Molecules and Their Contribution to Organic Aerosol in a Coastal City, Environ. Sci. Technol., 57, 15956–15967, https://doi.org/10.1021/acs.est.3c03244, 2023.
Yao, L., Garmash, O., Bianchi, F., Zheng, J., Yan, C., Kontkanen, J., Junninen, H., Mazon, S. B., Ehn, M., Paasonen, P., Sipilä, M., Wang, M., Wang, X., Xiao, S., Chen, H., Lu, Y., Zhang, B., Wang, D., Fu, Q., Geng, F., Li, L., Wang, H., Qiao, L., Yang, X., Chen, J., Kerminen, V.-M., Petäjä, T., Worsnop, D. R., Kulmala, M., and Wang, L.: Atmospheric new particle formation from sulfuric acid and amines in a Chinese megacity, Science (80-.)., 361, 278–281, https://doi.org/10.1126/science.aao4839, 2018.
Yuan, B., Chen, W., Shao, M., Wang, M., Lu, S., Wang, B., Liu, Y., Chang, C. C., and Wang, B.: Measurements of ambient hydrocarbons and carbonyls in the Pearl River Delta (PRD), China, Atmos. Res., 116, 93–104, https://doi.org/10.1016/j.atmosres.2012.03.006, 2012.
Zaytsev, A., Koss, A. R., Breitenlechner, M., Krechmer, J. E., Nihill, K. J., Lim, C. Y., Rowe, J. C., Cox, J. L., Moss, J., Roscioli, J. R., Canagaratna, M. R., Worsnop, D. R., Kroll, J. H., and Keutsch, F. N.: Mechanistic study of the formation of ring-retaining and ring-opening products from the oxidation of aromatic compounds under urban atmospheric conditions, Atmos. Chem. Phys., 19, 15117–15129, https://doi.org/10.5194/acp-19-15117-2019, 2019.
Zhao, Y., Thornton, J. A., and Pye, H. O. T.: Quantitative constraints on autoxidation and dimer formation from direct probing of monoterpene-derived peroxy radical chemistry, Proc. Natl. Acad. Sci., 115, 12142–12147, https://doi.org/10.1073/pnas.1812147115, 2018.